Low-rank-based residual statics estimation and correction

Alfaraj, Ali M.; Verschuur, D. J.; Herrmann, Felix J.

DOI
10.1190/GEO2022-0415.1

Publication date
2023

Document Version
Final published version

Published in
Geophysics

GEOPHYSICS, VOL. 88, NO. 3 (MAY-JUNE 2023); P. V215–V231, 22 FIGS., 2 TABLES.
10.1190/GEO2022-0415.1

DOI:10.1190/geo2022-0415.1

Low-rank-based residual statics estimation and correction

Ali M. Alfaraj[1], D. J. (Eric) Verschuur[1], and Felix J. Herrmann[2]

ABSTRACT

Surface consistency forms the basis for short-wavelength statics estimation. When raypaths in the near surface diverge from a normal incidence or when the normal moveout (NMO) velocity is inaccurate, surface-consistent methods may fail to estimate accurate statics. Existing nonsurface-consistent techniques can be prone to errors due to the need to construct pilot traces or pick horizons while imposing additional computational costs. To overcome these limitations and correct for the surface- and nonsurface-consistent statics, we have developed a low-rank-based residual statics (LR-ReS) estimation and correction framework. The method makes use of the redundant nature of seismic data by using its low-rank structure in the midpoint-offset-frequency domain. Due to the near-surface effect, the low-rank structure is destroyed. Therefore, we estimate the statics by means of low-rank approximation and crosscorrelation. To alleviate the need for accurate rank selection for low-rank approximation and improved statics estimation, we implement the method in an iterative and multiscale fashion. Because the low-rank approximation deteriorates at high frequencies, we use its better performance at low frequencies and exploit the common statics among the different frequency bands. The LR-ReS estimation and correction can be applied to data without an NMO correction, which makes statics estimation independent of the NMO velocity errors. Consequently, it can reduce the multiple iterations of the NMO velocity estimation and short-wavelength statics correction commonly needed for conventional methods to improve their performance. Moreover, the LR-ReS estimation does not require windowing of a noise-free area containing aligned primaries or mute to avoid the NMO stretch effect, which enables statics correction of the wavefield of all offsets. To evaluate the performance of our method, we apply it to simulated data and a challenging field data set affected by complex weathering layers and noise, which indicate a substantial improvement compared with conventional short-wavelength statics correction.

INTRODUCTION

Land seismic data sets often are challenged by near-surface weathering layers. They can lead to wave propagation effects that manifest themselves mostly as undesired time shifts, commonly called "statics" (Taner et al., 1974; Yilmaz, 2001). Although statics correction should be replaced by dynamic velocity analysis of the near surface as has been suggested by Ronen and Claerbout (1985) and Cox (1999), it is still a convenient way to overcome the limitations in the acquisition, velocity, and image estimation engines.

Due to rapid changes in surface elevation, the base of the weathering layers, and the weathering layers' velocity, land data are affected by short-wavelength (residual) statics (Yilmaz, 2001). Conventional short-wavelength statics correction methods rely on the surface-consistency assumption, where raypaths in the near surface are assumed to be vertical (Taner et al., 1974; Ronen and Claerbout, 1985; Marsden, 1993; Cox, 1999; Yilmaz, 2001). In this situation, the statics depend only on the locations of sources and receivers at the surface without considering their offsets. Sheriff (2002) argues that the surface-consistency assumption is not strictly correct. Cox (1999) further analyzes the assumption and concludes that it works in practice in most cases as surface-consistent statics are approximately equivalent to a simple near-surface model. Most surface-consistent methods estimate residual statics using normal moveout (NMO)-corrected common-midpoint (CMP) gathers (Yilmaz, 2001). The NMO correction should ideally remove the dynamic component related to the velocity such that the residual static

Manuscript received by the Editor 24 June 2022; revised manuscript received 14 December 2022; published ahead of production 1 February 2023; published online 12 April 2023.
[1]Delft University of Technology, Department of Imaging Physics, Delft, The Netherlands. E-mail: a.m.a.alfaraj@tudelft.nl (corresponding author); d.j.verschuur@tudelft.nl.
[2]Georgia Institute of Technology, School of Earth and Atmospheric Sciences, School of Computational Science and Engineering, Atlanta, Georgia, USA. E-mail: felix.herrmann@gatech.edu.

DOI:10.1190/geo2022-0415.1

component becomes more clear. In other words, surface-consistent methods assume that traces are aligned after NMO correction, and if they are not, then residual statics or residual NMO are the main causes. Moreover, it becomes easier to obtain a reference trace with less near-surface imprint from the presumably aligned traces after NMO correction. Other than NMO correction, surface-consistent residual statics correction methods require windowing of a noise-free area containing primaries because they are aligned reflections. However, short-wavelength statics also can lead to ambiguity during NMO velocity estimation. Therefore, multiple iterations of NMO velocity estimation and short-wavelength statics correction are usually carried out to improve their performance (Yilmaz, 2001), which can be effort- and time-consuming. Using migrated gathers, Xu et al. (2018) estimate surface-consistent statics. The method also needs an accurate velocity for migration, which can be computationally expensive. When the surface-consistency assumption is violated, errors in the estimated statics may arise, which calls for a nonsurface-consistent near-surface correction. Throughout the paper, the term "residual" statics is not only limited to surface-consistent statics but also nonsurface-consistent ones.

Henley (2012) proposes a framework that uses the common-angle domain based on raypath interferometry to correct for nonsurface-consistent statics. The method requires horizon picking and pilot-trace construction, which are not trivial tasks when the events picked are not continuous or in the presence of noise. Another type of nonsurface-consistent statics correction is trim statics, which is based on the crosscorrelation of individual traces with a model trace usually formed by stacking several CMP gathers (Cox, 1999). Ursenbach and Bancroft (2005) demonstrate the danger in aligning noise as a signal and describe it as "playing with fire." More recently, Breuer et al. (2020) use deep learning to estimate aligned events from unaligned ones by assuming that trim statics are the cause of unalignment. However, this approach may require accurate velocity as well as accurate knowledge of the primaries to avoid aligning multiples as primaries. Surface-consistent statics estimation methods also can be evaluated over multiple offset windows. This option, however, adds to the computational costs and decreases the number of traces in each offset window, which may lead to errors as a result of a low signal-to-noise ratio. The preceding methods still need access to an NMO velocity model, which can influence the estimated statics. In an alternative approach, one can process a seismic data set by exploiting its redundant nature, which allows for accurate low-rank approximation. When near-surface weathering layers influence the data's coherency, a rank-based solution can be used for statics correction.

Rank-based methods have been applied in different areas of seismic data processing, which date back to the 1980s (Ulrych et al., 1988). More recent examples include denoising (Bekara and Van der Baan, 2007; Trickett and Burroughs, 2009; Trickett et al., 2010; Moldoveanu, 2011; Chen et al., 2017; Zhang et al., 2020), interpolation (Trickett et al., 2010; Oropeza and Sacchi, 2011; Kreimer and Sacchi, 2012; Aravkin et al., 2014; Kumar et al., 2015), deblending (Maraschini et al., 2012; Wason et al., 2014; Cheng and Sacchi, 2015), and residual statics correction (Alfaraj et al., 2018, 2019). The common ground of these methods is that ideal seismic data in a transform domain, e.g., when organized as a matrix in the midpoint-offset domain, can be approximated by a low-rank matrix, whereas nonideal data, e.g., noisy or subsampled data, exhibit slowly decaying singular values. An alternative to rank is to use sparsity to compensate for short-wavelength statics. Gholami (2013) applies sparsity maximization in the Fourier domain on synthetic data and in the curvelet domain on field data due to the latter's better performance. However, the curvelet transform (Candes et al., 2006) can be computationally demanding. Stanton et al. (2013) modify projection onto convex sets to compensate for residual statics during interpolation in the Fourier domain. Similarly, Gholami (2014) uses phase retrieval to interpolate data affected by residual statics but uses only the amplitude spectrum and sparsity promoting regularization. To ensure sparsity, these methods may require data windowing, which may affect the estimated statics. Alfaraj et al. (2018, 2019) correct the statics by estimation of low-rank approximated data. Nonetheless, that method may suffer from amplitude losses, particularly at high frequencies, where the low-rank approximation is more challenging, leading to erroneous amplitude-variation-with-offset (AVO) responses. To circumvent the amplitude losses and preserve the AVO response, we use low-rank approximation as an intermediate step in statics estimation and correction.

Contributions

In a step toward more accurate short-wavelength statics correction, we diverge from the vertical raypath assumption in the near surface. We propose a novel low-rank-based residual statics (LR-ReS) estimation and correction framework. The method makes use of the redundant nature of seismic data, which allows for accurate approximation by low-rank matrices in the midpoint-offset domain. To estimate the statics, we cross-correlate a data set influenced by the near-surface weathering layers with its low-rank-approximated version. Because we estimate the statics and no longer the directly low-rank approximated data (as shown by Alfaraj et al., 2018, 2019), we can apply these statics to the original data and, thereby, preserve the AVO response. To mitigate the poor performance of low-rank approximation at high frequencies, we exploit the common statics among different frequency bands; we first use the low-frequency bands, where low-rank approximation performs better than high-frequency bands, to estimate the statics followed by statics correction of the full-band data. Because these statics are not sufficiently accurate for the total bandwidth, they are updated during statics estimation when including the high frequencies. To improve the estimated statics and to alleviate the need for accurate rank selection for low-rank approximation, we implement the method in an iterative and multiscale fashion.

The proposed method relaxes the surface-consistency assumption to estimate more accurate surface- and nonsurface-consistent statics at once. In practice, multiple steps are performed, where surface-consistent residual statics are first estimated followed by a brute-force nonsurface-consistent step, to account for both components. Moreover, the proposed method does not require NMO correction for short-wavelength statics estimation. Therefore, statics estimation becomes independent of errors in the NMO velocity model. Consequently, we can reduce the efforts- and time-consuming multiple passes of short-wavelength statics correction and NMO velocity estimation commonly needed for conventional methods to improve their performance. In addition, statics estimation and correction of the total wavefield without windowing to select aligned primaries or to avoid the NMO stretch effect become feasible. We demonstrate that the proposed method preserves the underlying structure's kinematic and dynamic properties while estimating accurate statics in a computationally efficient manner.

Outline

We first provide the reader with the requirements for the success of short-wavelength statics correction with a rank-based approach. We then describe the details of our proposed method, which we apply to synthetic data and a noisy field data set affected by complex weathering layers. We show the uplift we obtain compared with conventional methods on the CMP gathers, NMO velocity semblance, stack, AVO analysis, and automatic horizon picking. After that, we discuss the results within the context of NMO velocity estimation and data windowing, the method's practical aspects, its computational efficiency, improvement by mitigation of the noise effect, and further extensions and applications.

RANK-BASED PROCESSING PRINCIPLES

Rapid variations in surface elevation, the base of the weathering layers, and the weathering layers' velocity affect the data with short-wavelength statics (Yilmaz, 2001). As a result, the coherency of the data will decrease to result in slowly decaying singular values compared with the statics-free situation. To exploit the data's redundancy and correct for the weathering layers' effect, we need to estimate a low-rank matrix given that the desired statics-free data are of low-rank nature. With further elaboration, we define the main principles required to correct short-wavelength statics with a low-rank-based approach.

Simulated data

For the demonstration, we use synthetic data modeled with acoustic finite-difference modeling (Thorbecke and Draganov, 2011). The data's source and receiver intervals are 10 m and the maximum offset is 4 km. Figure 1 shows the velocity model we use to simulate the data displayed in the time and frequency domains in Figures 2a, 2c, 2e, and 3a–3d, respectively. To add short-wavelength statics, we shift each trace in each shot and receiver gather by up to ±52 ms, which is considerably larger than the usual residual statics (Figures 2b, 2d, 2f, 4a, and 4b). To mimic a realistic scenario, we design the statics to contain surface-consistent elements, where all traces recorded at the same shot or receiver location are assigned the same statics (up to ±40 ms) and nonsurface-consistent elements (up to ±20 ms).

Low-rank structure

Seismic data exhibit redundancy that can be exploited through their rank structure in the midpoint-offset (m-h) domain. Each midpoint m and offset h can be calculated from the source s and receiver r coordinates as follows, respectively:

$$m = \frac{s + r}{2} \tag{1a}$$

and

$$h = s - r. \tag{1b}$$

In the midpoint-offset domain, multiple raypaths sample the same CMP with different offsets (Figures 2d, 2e, 3b, and 3d). Moreover, it rotates the strong energy along the diagonal in the source-receiver (s-r) domain to the near-offset columns (Figure 3). Therefore, we expect the structure of statics-free data in the midpoint-offset domain to be of low-rank nature, i.e., low-rank structure corresponds to matrices that can be approximated by a low-rank matrix. The approximation can be achieved when the singular values decay rapidly, which enables their truncation. Given a constant frequency slice $\mathbf{X} \in \mathbb{C}^{n_m \times n_h}$ with complex entries of midpoints and offsets, where n_m and n_h correspond to the number of midpoints and offsets, respectively, we can compute its orthogonal decomposition by singular value decomposition (SVD) (Golub and Reinsch, 1971):

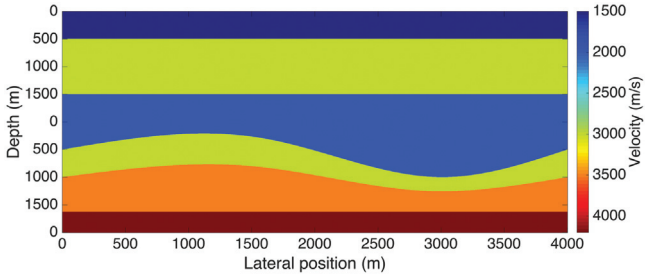

Figure 1. The velocity model used for synthetic data simulation.

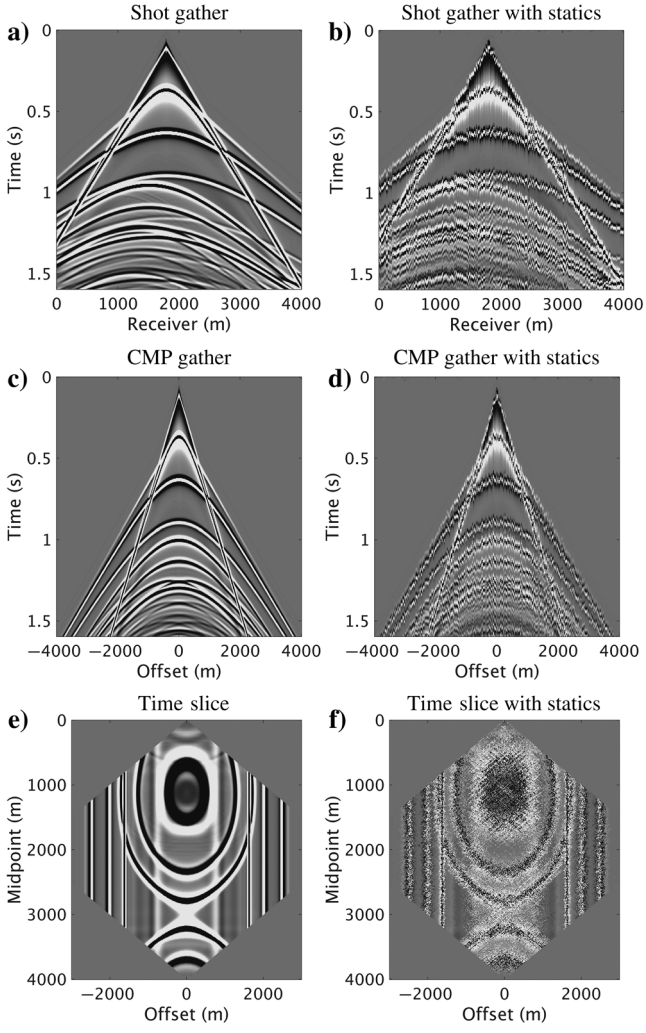

Figure 2. Simulated (a, c, and e) statics-free data and (b, d, and f) data after application of up to ±52 ms of surface- and nonsurface consistent statics. (a and b) Shot gathers, (c and d) CMP gathers, and (e and f) time slices at 1.0 s in the midpoint-offset domain.

DOI:10.1190/geo2022-0415.1

$$\mathbf{X} = \mathbf{U}\mathbf{S}\mathbf{V}^H, \tag{2}$$

where ^{H} denotes the Hermitian transpose and $\mathbf{U} \in \mathbb{C}^{n_m \times k}$ and $\mathbf{V} \in \mathbb{C}^{n_h \times k}$ are the orthogonal matrices holding the left and right singular vectors, respectively. The block diagonal matrix $\mathbf{S} \in \mathbb{R}^{k \times k}$ contains the nonnegative real-valued singular values, such that $\mathbf{S} = \text{diag}(s_1, s_2, s_3, \ldots, s_k)$, where $s_1 \geq s_2 \geq s_3 \geq \ldots \geq s_k \geq 0$ and $k = \min\{n_m, n_h\}$ is the rank of the frequency slice. For the matrix to exhibit a low-rank structure, the condition $k \ll \min\{n_m, n_h\}$ must be satisfied such that the singular values decay rapidly so they can be truncated for small k.

The low-rank structure can be exploited in different domains, where the domain of choice and subsequently the performance of the method depend on how rapidly the singular values of statics-free data decay. In addition to the potential midpoint-offset transform domain, we examine the acquisition (source-receiver) domain. We consider monochromatic frequency slices rather than time slices. The reason is that time slices contain more variability as they encompass all of the frequency ranges, which makes their low-rank approximation more difficult. On the contrary, low-rank approximation of low-frequency slices can be achieved with high accuracy. From the modeled statics-free data, we select frequency slices spanning relatively low to high frequencies and examine the decay of their singular values in the source-receiver and midpoint-offset domains (Figure 3). As expected, we observe that the singular values in the midpoint-offset domain decay more rapidly compared with those in the acquisition domain. This makes the former a better potential transform domain as it better satisfies the requirements of the first principle. Additional analysis of the singular values behavior of data affected by the near-surface weathering layers is required to confirm the potential of this transform domain.

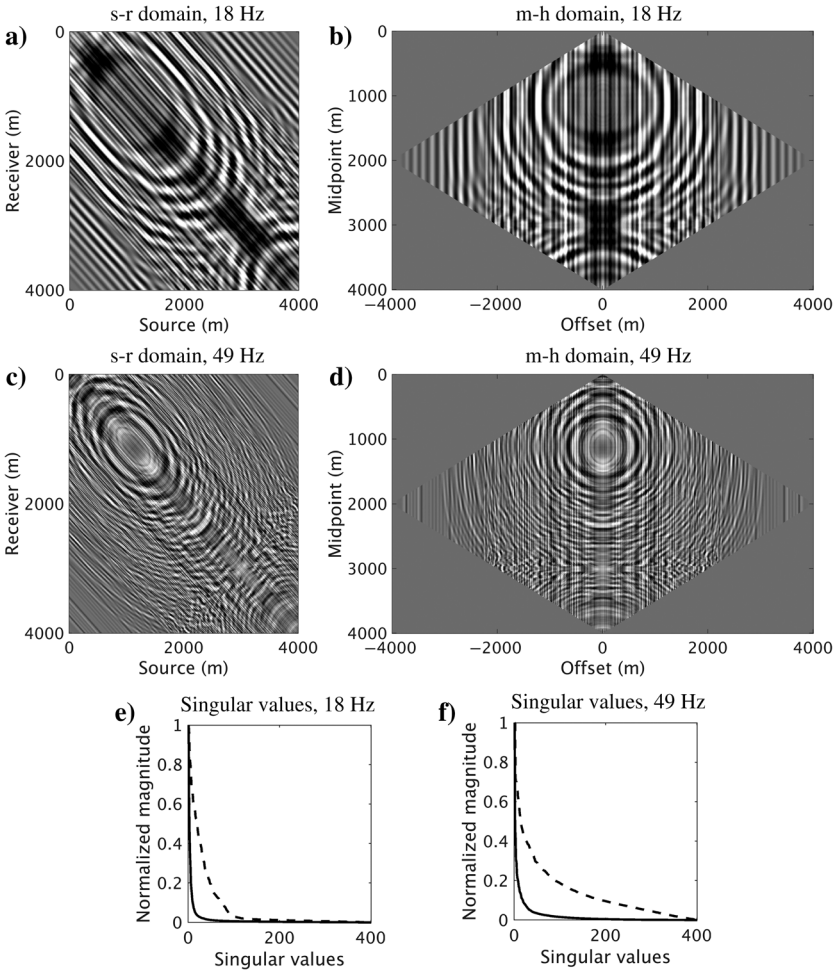

Figure 3. Statics-free frequency slices (the real part) and their singular values decay curves extracted from statics-free data at (a, b, and e) 18 Hz and (c, d, and f) 49 Hz in the (a and c) source-receiver domain and (b and d) midpoint-offset domain. The dashed lines in (e and f) the singular values decay curves indicate the source-receiver domain, whereas the solid lines correspond to the midpoint-offset domain.

Structure destruction

We rely on rapid variations in the near-surface weathering layers to destroy the low-rank structure. Due to short-wavelength statics, the data become less coherent, which leads to slowly decaying singular values. To analyze the resultant rank structure of data affected by the statics, we transform the data from the source-receiver domain to the midpoint-offset domain, where we can exploit the data's redundancy and compute the singular values of two frequency slices at relatively low and high frequencies (Figure 4). We observe that they are slower than those of statics-free data, which are more visible at higher frequencies as short-wavelength statics affect them more than the low frequencies. Because we satisfy the first and second principles using the midpoint-offset domain, we proceed with low-rank promotion to correct for short-wavelength statics.

Structure promotion

Due to the near-surface effects, the singular values become slowly decaying as they render coherent energy incoherent. Owing to the inherent redundancy of seismic data in the midpoint-offset-frequency domain, the largest singular values preserve the coherent energy, whereas the lower ones are related to the incoherency. Therefore, the low-rank approximation is one way to promote the low-rank structure to obtain a coherent signal without the near-surface imprint. Given a midpoint-offset frequency slice $\mathbf{Y} \in \mathbb{C}^{n_m \times n_h}$ selected from observed data, we can obtain a low-rank approximated matrix $\mathbf{X} \in \mathbb{C}^{n_m \times n_h}$ by solving the following rank-minimization problem:

$$\underset{\mathbf{X}}{\text{minimize}} \; \|\mathbf{X} - \mathbf{Y}\|_F \; \text{subject to} \; \text{rank}(\mathbf{X}) \leq k, \tag{3a}$$

where

$$\|\mathbf{X}\|_F = \sqrt{\sum_{i=1}^{n_m} \sum_{j=1}^{n_h} \mathbf{X}^{(ij)^2}} \tag{3b}$$

is the Frobenius norm that is equivalent to the ℓ_2 norm of a vector and $\mathbf{X}^{(ij)}$ is the ij-elements of $\mathbf{X}$. By imposing the constraint $k \ll \min\{n_m, n_h\}$, we restrict the solution $\mathbf{X}$ to be of a low-rank nature, which can be found through the SVD (Eckart and

Young, 1936). Trickett and Burroughs (2009) suppress random noise with the eigenimage and Cadzow filtering, where the former is more applicable to 3D stacked traces (Trickett, 2003). Moldoveanu (2011) uses SVD to attenuate swell noise. The method proposed by Alfaraj et al. (2018, 2019), which requires NMO velocity estimation, suggests that, by selecting a small number of singular vectors corresponding to the few largest singular values, one can obtain an estimate of $\mathbf{Y}$ without the imprint of short-wavelength statics. Because we have shown that the rank-based processing principles can be satisfied without NMO correction, we modify that method to correct for residual statics with a low-rank approximation (Algorithm 1).

The input to Algorithm 1 is data $\mathbf{D}_{sr}$ in the time-source-receiver domain, where n_t, n_s, and n_r correspond to the number of time, source, and receiver samples, respectively (Figure 2b), and rank k for each frequency slice. Throughout the algorithm, the subscripts and superscripts $_{sr}$, $_{mh}$, $_{lr}$, $\tilde{}$, and $\hat{}$ indicate the source-receiver domain, midpoint-offset domain, low-rank approximated data, frequency domain, and output estimated data, respectively. We first transform the data $\mathbf{D}_{sr}$ from the source-receiver domain to the midpoint-offset domain, where we can exploit the data's redundancy to obtain $\mathbf{D}_{mh}$ (Figure 2d). We then use fast Fourier transform (FFT) to transform the data to the frequency domain to obtain $\tilde{\mathbf{D}}_{mh}$ (Figure 4a and 4b) as indicated by the second step of the algorithm. After that, there is a loop over frequencies (step 3), where the singular values of the frequency slices are calculated (step 4). In the fifth step, where $\mathbf{u}^{(j)}$ and $\mathbf{v}^{(j)}$ correspond to the jth columns of the matrices $\mathbf{U}$ and $\mathbf{V}$ of equation 3, respectively, the data below the rank threshold level k are neglected (Figure 5c and 5d). Here, $\tilde{\mathbf{D}}_{lr} \in \mathbb{C}^{n_m \times n_h \times n_f}$ is the estimated low-rank data from all of the frequencies in the midpoint-offset domain, which can be transformed by inverse fast Fourier transform (IFFT) to obtain the low-rank approximated data in the time domain $\hat{\mathbf{D}}_{lr}$ as indicated by the sixth step (Figure 5a and 5b).

At low frequencies, low-rank approximation can reduce the effect of statics, as shown by the time- and low-frequency slices in Figure 5b and 5c, respectively, compared with those of data with statics (Figures 2f and 4a). However, there is a dimming in the data's amplitude after low-rank approximation. The second hurdle is that, at high frequencies, the data contain more variability whereas the influence of the near surface can be stronger (Figure 4). Consequently, the performance of low-rank approximation deteriorates, resulting in noisy data (Figure 5a and 5d). To avoid low-rank approximation errors at low and high frequencies, we propose the following iterative and multiscale framework.

LR-RES ESTIMATION AND CORRECTION

Our proposed method uses the properties of the midpoint-offset domain, where short-wavelength statics lead to slowly decaying singular values, whereas statics-free frequency slices are of low-rank nature (Figure 4c and 4d). By imposing the low-rank constraint, we can obtain frequency slices with less statics imprint. Although they may contain amplitude losses due to inaccurate low-rank approximation, we can use the low-rank approximation as an intermediate step to estimate the statics. To tackle the poor performance of low-rank approximation at high frequencies, we use its better performance at low frequencies and exploit the similarity in the statics' influence among multiple frequency bands. For improved statics estimation and to alleviate the need for accurate rank selection, which is required for low-rank approximation, we implement the framework in an iterative and multiscale fashion. The proposed method uses parts of Algorithm 1 as building blocks for short-wavelength statics estimation and correction, as detailed in Algorithm 2.

The LR-ReS estimation and correction algorithm contains the same preprocessing steps of Algorithm 1 (steps 1 and 2). Similarly, Algorithm 2 includes a loop over frequency slices, where f_{min} and f_{max} are, respectively, the minimum and maximum frequencies we loop over (step 4). As is the case for Algorithm 1, Algorithm 2

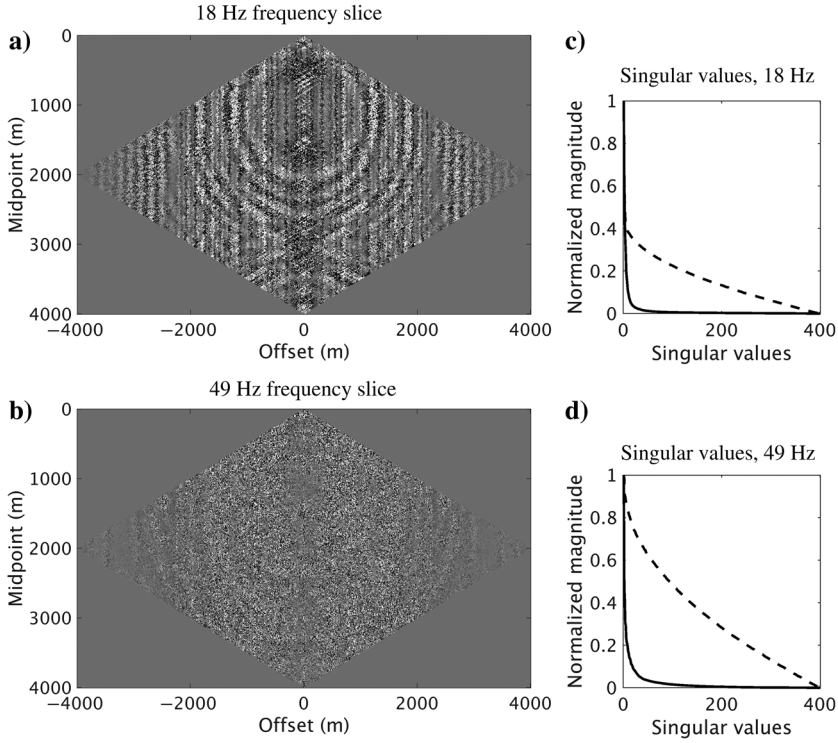

Figure 4. Frequency slices of synthetic data affected by up to ±52 ms of short-wavelength statics at (a) 18 Hz and (b) 49 Hz in the midpoint-offset domain along with (c and d) their singular values decay curves, respectively, in the dashed lines. They are slowly decaying compared with those of the statics-free data (Figure 3b and 3d) repeated here in solid lines.

Algorithm 1. Low-rank approximation.

Input: $\mathbf{D}_{sr} \in \mathbb{R}^{n_t \times n_r \times n_s}$ and $\mathbf{k} \in \mathbb{R}^{n_f}$
Output: $\hat{\mathbf{D}}_{lr} \in \mathbb{R}^{n_t \times n_h \times n_m}$
1. Transform $\mathbf{D}_{sr}$ to $\mathbf{D}_{mh} \in \mathbb{R}^{n_t \times n_h \times n_m}$ with equation 1
2. FFT $\mathbf{D}_{mh}$ to $\tilde{\mathbf{D}}_{mh} \in \mathbb{C}^{n_m \times n_h \times n_f}$
3. **for** $f \leftarrow 1$ **to** n_f **do**
4. Calculate SVD for $\tilde{\mathbf{D}}_{mh}^{(f)}$ with equation 2
5. $\tilde{\mathbf{D}}_{lr}^{(f)} \leftarrow \sum_{j=1}^{k^{(f)}} s^{(j)} \mathbf{u}^{(j)} \mathbf{v}^{(j)H}$
6. IFFT $\tilde{\mathbf{D}}_{lr}$ to $\hat{\mathbf{D}}_{lr}$

DOI:10.1190/geo2022-0415.1

involves the calculation of the singular values and the approximation of low-rank data as indicated by steps 5 and 6, respectively. Figure 6b and 6e shows that low-rank approximation at low frequencies is capable of reducing the imprint of statics compared with the low-pass-filtered data affected by statics (Figure 6a and 6d). At the same time, these figures demonstrate that low-rank approximation results in the reduction of the data's amplitude due to neglecting data of importance. To preserve the AVO response, we avoid the use of the low-rank approximated data as the final solution. We instead estimate the statics $\mathbf{T}_{\text{mh}}$ by the cross-correlation of the data with statics $\underline{\mathbf{D}}_{\text{mh}}$ (Figure 6a and 6d) and low-rank approximated data $\mathbf{D}_{\text{lr}}$ (Figure 6b and 6e) along the time dimension in the midpoint-offset domain (steps 7–10). Note that $\underline{\mathbf{D}}_{\text{mh}}$ (Figure 6a and 6d) is a band-pass-filtered version of the data with statics $\mathbf{D}_{\text{mh}}$ (Figure 2d and 2f). The estimated statics can then be used for statics correction of the full-band data $\mathbf{D}_{\text{mh}}$ to obtain statics-corrected data $\hat{\mathbf{D}}_{\text{mh}}$ (step 11). Figure 6c and 6f displays the data after partial statics correction with statics estimated from the low frequencies, which is already an improvement compared with the input (Figure 2d and 2f).

Algorithm 2. LR-ReS estimation and correction.

Input: $\mathbf{D}_{\text{sr}} \in \mathbb{R}^{n_t \times n_r \times n_s}$, $\mathbf{K} \in \mathbb{R}^{n_f \times n_l}$, $\mathbf{f_b} \in \mathbb{R}^{n_{f_b}}$, $f_{\min} \in \mathbb{R}$, $f_{\max} \in \mathbb{R}$
Output: $\hat{\mathbf{D}}_{\text{mh}} \in \mathbb{R}^{n_t \times n_h \times n_m \times n_l}$, $\mathbf{T}_{\text{mh}} \in \mathbb{R}^{n_h \times n_m \times n_l \times n_{f_b}}$, $\hat{\mathbf{D}}_{\text{sr}} \in \mathbb{R}^{n_t \times n_r \times n_s}$, and $\mathbf{T}_{\text{sr}} \in \mathbb{R}^{n_r \times n_s}$

1. Transform $\mathbf{D}_{\text{sr}}$ to $\mathbf{D}_{\text{mh}} \in \mathbb{R}^{n_t \times n_h \times n_m}$ with equation 1
2. FFT $\mathbf{D}_{\text{mh}}$ to $\tilde{\mathbf{D}}_{\text{mh}} \in \mathbb{C}^{n_m \times n_h \times n_f}$
3. **for** $l \leftarrow 1$ **to** n_l **do**
4. **for** $f \leftarrow f_{\min}$ **to** $f_{\max}$ **do**
5. Calculate SVD for $\tilde{\mathbf{D}}_{\text{mh}}^{(f)}$ with equation 2
6. $\tilde{\mathbf{D}}_{\text{lr}}^{(f)} \leftarrow \sum_{j=1}^{\mathbf{K}^{(f,l)}} s^{(j)} \mathbf{u}^{(j)} \mathbf{v}^{(j)H}$
7. **if** f is contained within $\mathbf{f_b}$ **then**
8. $i \leftarrow$ frequency-band index
9. IFFT $\tilde{\mathbf{D}}_{\text{lr}}$ to $\mathbf{D}_{\text{lr}}$, IFFT $\tilde{\mathbf{D}}_{\text{mh}}$ to $\underline{\mathbf{D}}_{\text{mh}}$
10. $\mathbf{T}_{\text{mh}}^{(l,i)} \leftarrow \mathcal{C}(\underline{\mathbf{D}}_{\text{mh}}, \mathbf{D}_{\text{lr}})$
11. $\hat{\mathbf{D}}_{\text{mh}}^{(l)} \leftarrow \tau(\mathbf{D}_{\text{mh}}, \mathbf{T}_{\text{mh}}^{(l,i)})$
12. $\mathbf{D}_{\text{mh}} \leftarrow \hat{\mathbf{D}}_{\text{mh}}^{(l)}$, FFT $\mathbf{D}_{\text{mh}}$ to $\tilde{\mathbf{D}}_{\text{mh}}$
13. Transform $\sum_{l=1}^{n_l} \sum_{i=1}^{n_{f_b}} \mathbf{T}_{\text{mh}}^{(l,i)}$ to $\mathbf{T}_{\text{sr}}$
14. $\hat{\mathbf{D}}_{\text{sr}} \leftarrow \tau(\mathbf{D}_{\text{sr}}, \mathbf{T}_{\text{sr}})$

Although low-rank approximation at low frequencies is sufficiently accurate for statics estimation, its performance deteriorates at high frequencies (Figure 5). To mitigate the poor low-rank approximation performance at high frequencies, we exploit the common statics among multiple frequency bands $\mathbf{f_b}$, i.e., we use the similarity in the statics' influence on multiple frequencies. To do so, we first estimate the statics from low-frequency bands (Figure 6a, 6b, 6d, and 6e) followed by a statics correction of the full-band data (Figure 6c and 6f). By applying the statics estimated at lower frequencies to the full-band data, we already increase the redundancy of higher-frequency slices because they share common statics with lower frequencies. Consequently, the low-rank approximation of higher frequencies are improved, which can be observed when comparing low-rank approximation after processing all of the frequencies (Figure 5a and 5b) to that obtained after statics estimation and correction using two frequency bands starting from low frequencies (Figure 7b and 7e). The latter figures show less statics imprint, less noise, and higher-frequency content when compared with the former. Because the statics estimated from low- or mid-frequency bands are not sufficiently accurate for the high frequencies (Figure 6c and 6f), they are updated when estimating the statics at high-frequency bands (Figure 7c and 7f). Compared with statics estimation and correction after processing each frequency slice, our proposed approach makes the algorithm more stable by avoiding spurious statics due to low-rank approximation errors or due to missing or corrupted frequencies, e.g., in the case of a low signal-to-noise ratio.

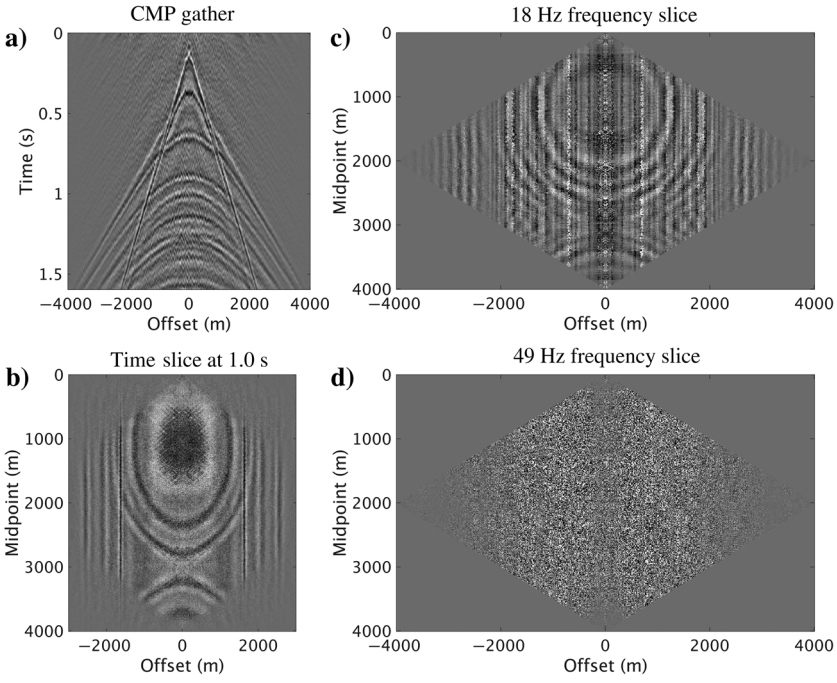

Figure 5. Residual statics correction with a low-rank approximation (Algorithm 1): (a) CMP gather and (b) time slice at 1.0 s and frequency slices at (c) 18 Hz and (d) 49 Hz in the midpoint-offset domain.

Therefore, when the loop over frequencies reaches the desired frequency band for statics estimation (step 7), we inverse Fourier transform the data with statics $\tilde{\mathbf{D}}_{\text{mh}}$ and low-rank approximated data $\tilde{\mathbf{D}}_{\text{lr}}$ (step 9) to the time domain (Figure 6a, 6b, 6d, and 6e, respectively). Note that $\mathbf{f_b}$ contains the maximum frequency of each frequency band. To estimate the statics, we then perform a crosscorrelation along the time dimension to find the lag corresponding to the largest crosscorrelation coefficient, which is indicated by the operator $\mathcal{C}$ (step 10). Let $\underline{\mathbf{d}}_{\text{mh}}$ and $\mathbf{d}_{\text{lr}} \in \mathbb{R}^{n_t}$ be traces extracted from data with statics $\underline{\mathbf{D}}_{\text{mh}}$ and low-rank approximated data $\mathbf{D}_{\text{lr}}$, respectively, and the estimated statics t_{mh} from these two traces can be found by

$$t_{\text{mh}} = \arg\max_{t} (\underline{\mathbf{d}}_{\text{mh}}(t) \star \mathbf{d}_{\text{lr}}(t)), \qquad (4)$$

where $\star$ indicates a crosscorrelation. After processing each frequency band, we apply equation 4 to all the traces to obtain the statics in the midpoint-offset domain $\mathbf{T}_{\text{mh}} \in \mathbb{R}^{n_m \times n_h}$. To correct for the statics, we shift each trace as indicated by the operator τ (step 11):

$$\hat{\mathbf{d}}_{\text{mh}} = \mathbf{d}_{\text{mh}}(t + t_{\text{mh}}), \tag{5}$$

where $\mathbf{d}_{\text{mh}}$ is a trace extracted from the full-band data with statics $\mathbf{D}_{\text{mh}}$. Figure 8a displays the estimated statics $\mathbf{T}_{\text{mh}}$ from all of the frequency bands at the first iteration, which we use for statics correction to obtain the estimated data (Figure 7c and 7f). The improvement also can be noticed when comparing the low- and high-frequency slices after the LR-ReS estimation and correction at this stage (Figure 9a and 9b) to the input frequencies (Figure 4a and 4b). However, there are still unresolved statics.

To improve the statics estimation and correction, the proposed algorithm contains an iterative loop over rank scales n_l (step 3), i.e., multiple ranks for the same frequency slice, which are required for a low-rank approximation (step 6). As a result, the input rank $\mathbf{K} \in \mathbb{R}^{n_f \times n_l}$ of Algorithm 2 becomes not only a function of frequency f as it was the case for Algorithm 1 but also rank scale l. By using a multi rank-scale approach, whereby we start with a relatively high rank and reduce it further with the number of iterations, we gradually extract multiscale time shifts. The reason we lower the rank is that the singular values decay faster as iterations progress, which we further elaborate on in the next paragraph. Figure 8a shows that most of the statics are estimated at the first rank-scale iteration, which are further fine-tuned at the second and third iterations of Algorithm 2 (Figure 8b and 8c, respectively). Even though the first scale eliminates the bulk of the statics, which leads to considerable improvements, it is still insufficient to account for all the statics. After two multiscale iterations, the frequency slices (Figure 9c–9f) and their singular values decay (Figure 10b and 10d) and time-domain data (Figure 11e and 11f) become similar to the statics-free ones (Figures 2c, 2e, 3b, and 3d). An additional benefit of using a multi-rank-scale approach is to reduce the need for accurate low-rank approximation, i.e., if the chosen rank is inadequate to compensate for all the statics at the first iteration, fine-tuning can be carried out at later iterations to improve the estimated statics and data.

We choose $\mathbf{K}$ according to the singular-value decay relations described in the "Rank-based processing principles" section. Because the frequency slices with short-wavelength statics exhibit low coherency, their singular values are characterized by slow decay (Figure 4c and 4d). Statics correction makes low-rank approximation more accurate as it maps the incoherent energy in the tail of the singular values to the coherent energy captured by the first singular values. In other words, the singular-value decay of the same frequency slice becomes more rapid after partial statics correction due to the improved coherency, which can be seen from the singular values decay curves after the first rank-scale iteration compared with those prior to the statics correction (Figure 10a and 10c). Because the singular values decay rapidly after applying the partial statics correction, we can use a lower rank at the next iteration to capture the coherent energy and neglect the incoherent one. The further the iterations progress, the faster the singular values will decay, which can be seen through the comparison of Figure 10a–10d.

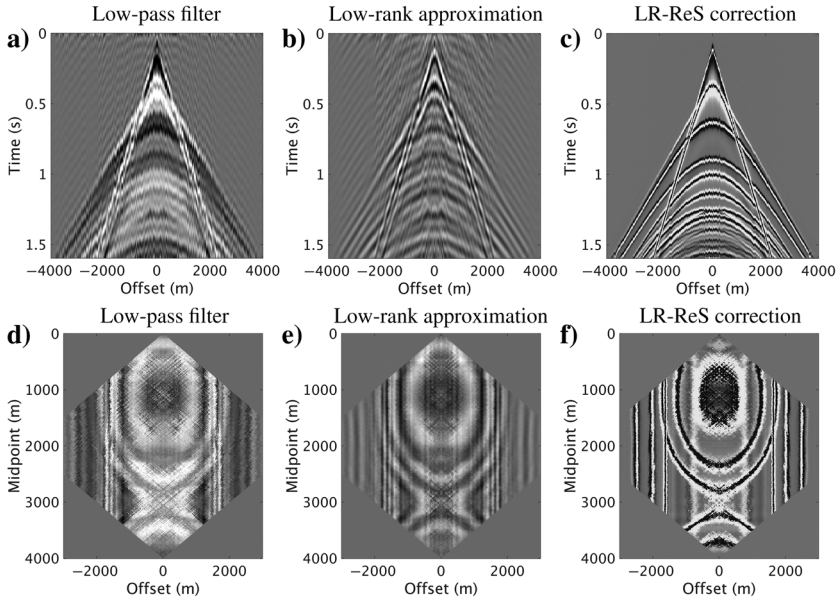

Figure 6. (a–c) CMP gathers and (d–f) time slices at 1.0 s extracted from (a and d) low-pass-filtered data with statics $\mathbf{D}_{\text{mh}}$, (b and e) low-rank approximated data $\mathbf{D}_{\text{lr}}$, and (c and f) statics-corrected data at the first frequency-band and first rank-scale iteration.

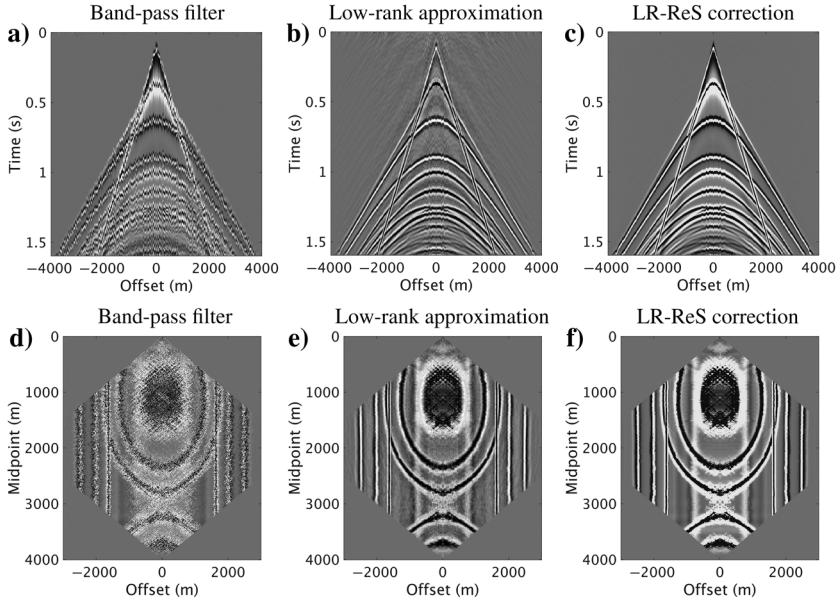

Figure 7. (a–c) CMP gathers and (d–f) time slices at 1.0 s extracted from (a and d) band-pass-filtered data with statics $\mathbf{D}_{\text{mh}}$, (b and e) low-rank approximated data $\mathbf{D}_{\text{lr}}$, and (c and f) statics-corrected data at the third frequency-band and the first rank-scale iteration.

Accordingly, we start the first rank-scale iteration with a relatively higher-rank approximation and decrease it further at later iterations. This is the opposite of other rank-based methods used, for example, in data interpolation, which needs to fill in the missing gaps with accurate amplitudes. In that case, the smaller singular values need to be preserved as they also contain important information to obtain accurate data. On the other hand, the LR-ReS estimation and correction seek to capture coherent energy, which can be obtained from low-rank approximated data. Since a low-rank version of the data can be inaccurate (Algorithm 1), we avoid using it as the final solution. We mitigate the inaccuracy of low-rank approximation with statics estimation (Algorithm 2), i.e., we implicitly use low-rank approximation to estimate the statics (time shifts), which we then apply to original data. Therefore, we preserve the amplitudes.

When the largest singular values represent the signal of interest, low-rank approximation preserves the predominant features of the signal. As a result, cross-correlating a low-rank version of the data with its full-rank one can be used to estimate the statics that enhance the signal. On the other hand, when the data are influenced by undesired events, e.g., the coherent noise or residual coherent noise, that span the largest singular values, initial rank-scale iterations can provide better statics estimation because they still preserve the signal. Because the algorithm outputs the multiscale statics $\mathbf{T}_{mh}$ and data $\hat{\mathbf{D}}_{mh}$, the user can quality control (QC) the results.

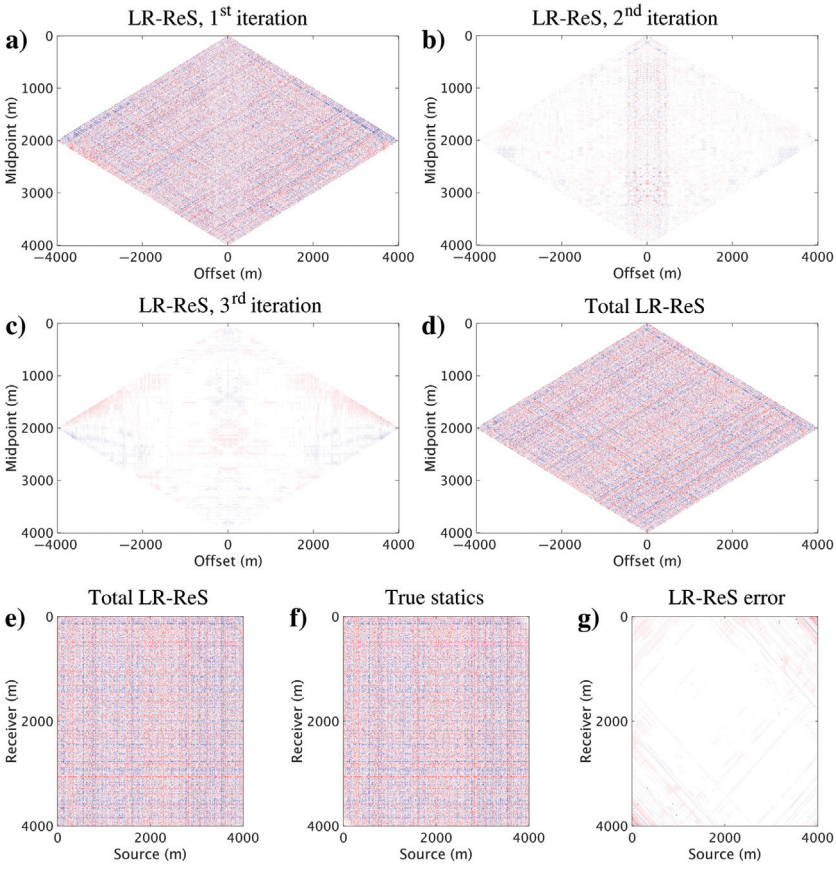

Figure 8. The estimated statics in the midpoint-offset domain at the (a) first, (b) second, and (c) third rank-scale iterations. The total estimated statics in the (d) midpoint-offset domain and (e) source-receiver domain. (f) The true statics and (g) the LR-ReS estimation error. The figures are clipped to ±52 ms.

At the end of the iterations over the frequencies and rank scales, the total midpoint-offset dependent statics $\mathbf{T}_{mh}$ (Figure 8d) can be transformed to the source-receiver domain to obtain $\mathbf{T}_{sr}$ (Figure 8e) as indicated by the 13th step of Algorithm 2. When compared with the actual nonsurface-consistent statics originally applied to the data (Figure 8f), the error of the LR-ReS displayed in Figure 8g is minimal. The estimated statics for one shot gather is shown in Figure 11h, where the error compared with the actual nonsurface-consistent statics is low. By applying $\mathbf{T}_{sr}$ to the input data $\mathbf{D}_{sr}$ (step 14), we estimate statics-corrected data in the source-receiver domain $\hat{\mathbf{D}}_{sr}$ (Figure 11d) that are of minimal discrepancy compared with the statics-free data (Figure 2a). Because the only difference between the input and output (Figures 2b and 11d, respectively) is statics correction, we are certain to preserve the AVO response. We note that if only surface-consistent statics are desired, e.g., when raypaths in the near surface are vertical to satisfy the surface-consistency assumption, they can be obtained by averaging along rows and columns of the estimated LR-ReS in the source-receiver domain $\mathbf{T}_{sr}$.

With our approach, we are assuming that the estimated time shifts are solely due to the near-surface effect. Because the dynamic component, e.g., data moveout, tends to be preserved in the largest singular values, it should not be affected. This can be illustrated when comparing, respectively, the input, output, and statics-free data displayed in the source-receiver domain (Figures 2a, 2b, and 11d) and midpoint-offset domain (Figures 2d, 2e, and 11e).

RESULTS

To further illustrate the potential of our proposed LR-ReS estimation and correction, we evaluate its performance in enhancing the data, stack, NMO velocity semblance, AVO analysis, and automatic horizons picking. We first show additional results of the synthetic data, followed by the application to field data. The results will be compared with conventional residual statics correction.

Synthetic data example

One of the popular short-wavelength statics correction methods is residuals statics correction with stack power maximization (SPM) (Ronen and Claerbout, 1985), which requires NMO velocity estimation, windowing over the noise-free area containing aligned primaries, and windowing to avoid the NMO stretch effect. Recently, Dukalski et al. (2022) use quantum annealing to improve the convergence of SPM to a global optimum. When applying the residual statics estimated with SPM to the synthetic data displayed in Figure 2b, 2d, and 2f, it provides suboptimal results because it only accounts for the surface-consistent statics (Figure 11a–11c). Figure 11g displays the estimated statics with SPM and their error compared with the total nonsurface-consistent statics, which is high, and only the surface-consistent component, which is lower. This can

be seen from the midpoint-offset domain time slice (Figure 11c), where the surface-consistent statics on the diagonals at 45° have been minimized compared with the time slice of the data with statics (Figure 2f). In this case and in similar situations in practice, where surface-consistent short-wavelength statics correction methods fail to resolve all the statics, an additional nonsurface-consistent solution is required. On the contrary, LR-ReS estimation and correction (Algorithm 2), which does not require either NMO velocity estimation or data windowing, is capable of accounting for the surface- and nonsurface-consistent statics to provide improved results (Figure 11d–11f) that resemble the statics-free data (Figure 2a, 2c, and 2e).

In the presence of short-wavelength statics, NMO-corrected CMP gathers result in distorted and low-resolution subsurface structures as they stack out of phase (Figure 12b), contrary to the statics-free data (Figure 12a). Residual statics correction with SPM increases the stack's resolution compared with one of the data with statics (Figure 12d). However, because it fails to fully correct for short-wavelength statics, the stack's resolution is not optimal as is evident from the computed average amplitude spectrum (Figure 12e). Using our proposed method, we obtain an undistorted and a higher resolution stack that is similar to the one obtained from the statics-free data (Figure 12c), which also is confirmed by the amplitude spectrum (Figure 12e). For additional quantitative analysis, we compute the average stack power p given by

$$p = \frac{1}{n_t}\sum_{t=1}^{n_t} |s(t)|^2, \tag{6}$$

which corresponds to the average sum of the absolute squares of a stacked trace $s(t)$ at each CMP. Relative to the statics-free stack, the average stack power of all the CMP gathers of the data with statics is 0.27. After residual statics correction with SPM, it becomes 0.45, whereas it is 0.96 after our proposed method.

A QC of residual statics can be performed by an analysis of the CMP gathers and their stacks, which shows that our proposed method preserves the structure and its amplitudes. Additional analyses are usually performed on the NMO velocity semblance (see the next paragraph) and the stack of the receiver or shot gathers. The latter also is used to ensure that the original structure does not change. Figure 13 shows the results of shot-gather stacks. The conclusions are similar to those inferred from the CMP stacks, where the LR-ReS does not introduce erroneous structures while accounting for most of the statics (Figure 13c), when compared with the statics-free case (Figure 13a). On the other hand, the surface-consistent statics estimated by SPM require an additional nonsurface-consistent statics correction step (Figure 13d). If the used window partly includes unaligned multiples, SPM introduces erroneous structures (Figure 13e), which demonstrates its dependence on optimal window selection and accurate NMO velocity estimation.

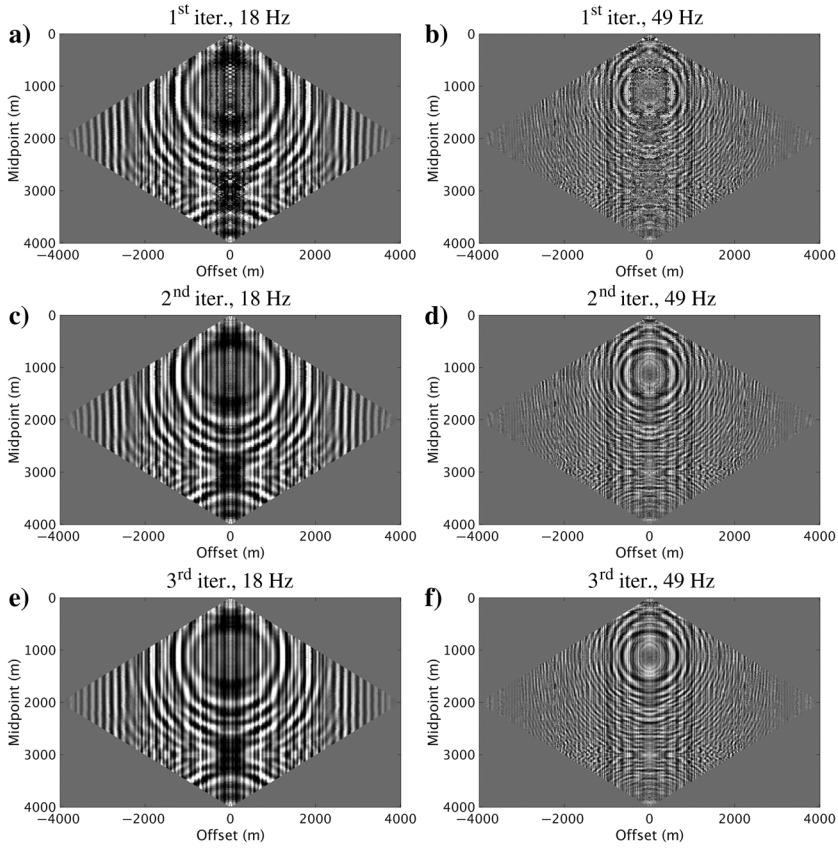

Figure 9. Frequency slices after the LR-ReS estimation and correction at the (a and b) first, (c and d) second, and (e and f) third rank-scale iterations of (a, c, and e) 18 Hz and (b, d, and f) 49 Hz.

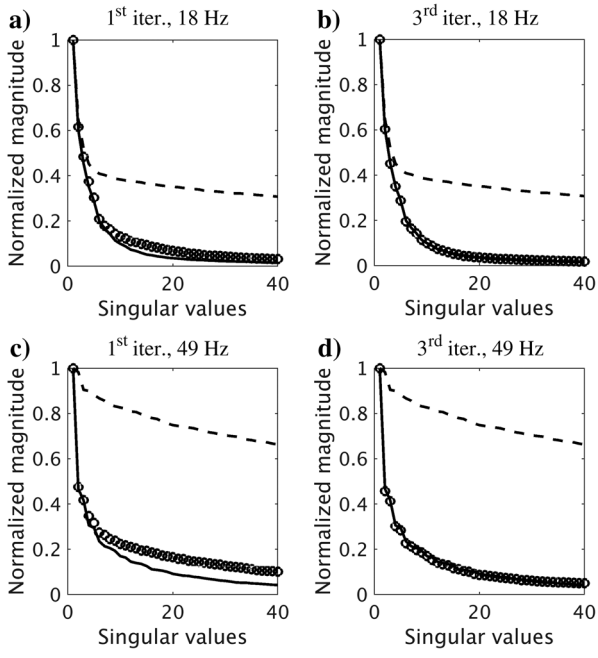

Figure 10. The largest singular values of (a and b) 18 Hz and (c and d) 49 Hz frequency slices of data with statics (Figure 4a and 4b) plotted in the dashed curves, statics-free data (Figure 3b and 3d) plotted in the solid curves, and after the LR-ReS correction at the (a and c) first (Figure 9a and 9b) and (b and d) third rank-scale iterations (Figure 9e and 9f) plotted in the circle markers.

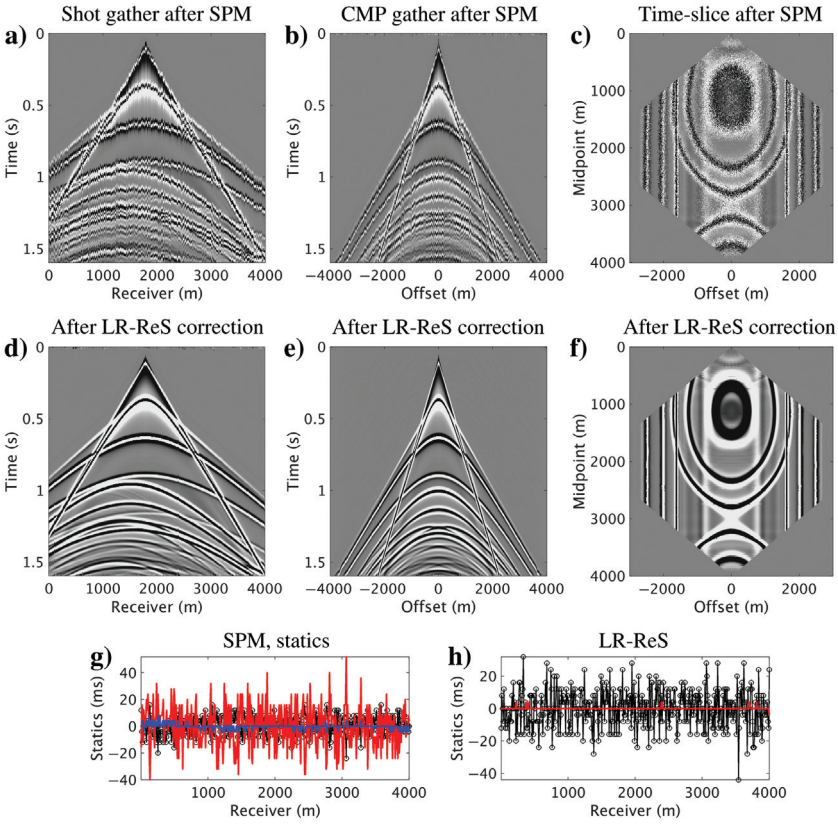

Figure 11. The estimated (a and d) shot gathers, (b and e) CMP gathers, (c and f) time slices in the midpoint-offset domain, and (g and h) source statics of (a and d) plotted in black along with their error in red after (a, b, c, and g) SPM residual statics correction and (d, e, f, and h) our proposed method. The blue line represents the error of SPM with respect to only the surface-consistent statics.

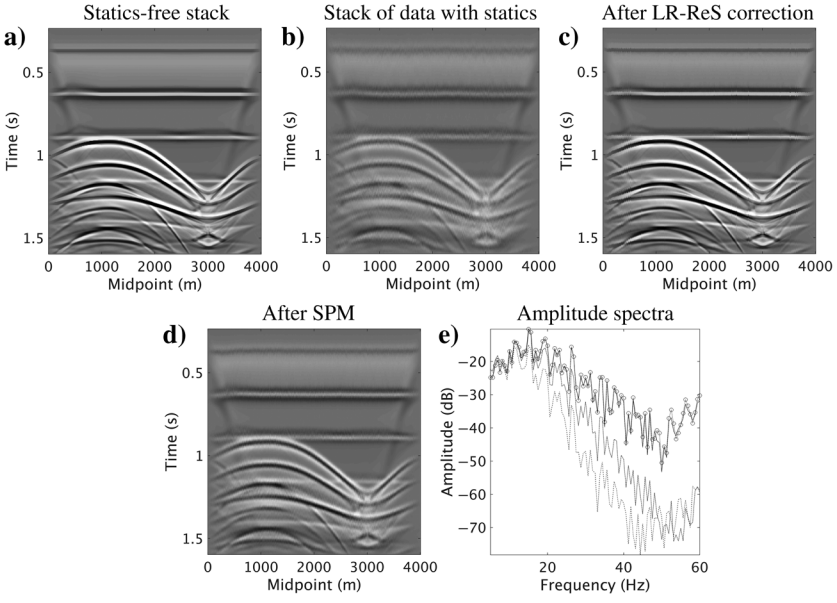

Figure 12. CMP stacks of (a) statics-free data and (b) data affected by short-wavelength statics and data after statics correction with (c) LR-ReS and (d) SPM. (e) The average amplitude spectra computed from (a–d) drawn in the dotted lines with circle markers, the dashed line, the solid line, and the dashed-dotted line, respectively.

Another important role for short-wavelength statics correction is improving the NMO velocity estimation, where both steps are usually applied in a flip-flop mode to improve their performance (Yilmaz, 2001). The semblance after LR-ReS estimation and correction, which is independent of the NMO velocity model, leads to less ambiguity and more confidence in picking the velocity similar to the statics-free situation (Figure 14a and 14c, respectively). Due to the influence of the statics, the resolution of the semblances obtained from the data with statics and after the SPM residual statics correction is suboptimal, which can result in ambiguity during the velocity picking process (Figure 14b and 14d).

Due to the importance of amplitude fidelity, we examine whether the LR-ReS estimation and correction can preserve the AVO response. Because the only difference between the output and the input is statics correction (Algorithm 2), we do not expect to change the amplitude values. However, the AVO analysis can be influenced when traces are unbalanced in the presence of residual statics (Chopra and Castagna, 2014). This can be seen in Figure 15, where the autopicked amplitudes of the horizon at 0.65 s from CMP gathers with statics and after SPM suffer from erroneous picks. In contrast, the autopicked amplitudes on the CMP gather after LR-ReS estimation and correction resemble those of statics-free data. When computing the AVO intercepts and gradients from all the CMP gathers at the same horizon, the statics-free data and the data after our proposed method provide a highly similar trend confined to the same area (Figure 15f). However, the intercepts and gradients computed from the CMP gathers with statics show a highly scattered trend. It becomes slightly improved after residual statics correction with SPM, but still unsatisfactory due to the effect of the unresolved statics. To this extent, the LR-ReS estimation and correction framework has shown its potential in correcting for the surface- and nonsurface-consistent short-wavelength statics on simulated data. To further evaluate its performance, we apply it to field data.

Field data example

The challenging field data set we consider for the demonstration is affected by complex near-surface weathering layers (Al-Ali and Verschuur, 2006). The data's source and receiver intervals are 30 m and the maximum offset is 3585 m. Figure 16d shows the surface elevation variation across the section. The topography also varies widely and includes gravel, loose sand, fast carbonates, and karsts. These conditions lead to the low-quality data and stack shown in Figures 16a and 17a, respectively. We apply minimal preprocessing on the data, which includes

elevation statics correction and frequency-wavenumber (*f-k*) filter for ground-roll attenuation. Figures 17a and 18a display five of the CMP gathers after preprocessing and after NMO correction, respectively, which clearly show the near-surface effect on the noncontinuous reflections. The data also contain near-offset noise, random noise, and residual ground roll. Unfortunately, residual statics correction with SPM results in minimal improvement (Figure 18c). The limited performance can be attributed to the violation of the surface-consistency assumption due to the complexity of the near-surface weathering layers that can lead to nonvertical raypaths in the near surface. To overcome the limitations of conventional residual statics correction, we apply our proposed method to this challenging field data set.

By using the proposed LR-ReS estimation and correction framework, we avoid the assumption that requires raypaths in the near surface to be vertical. This makes the method suitable for these data given the complexity of the near surface. As previously mentioned, we use three-rank scale iterations and three frequency bands within the available frequency content (10.5–58 Hz). Figure 17b displays the CMP gathers after the LR-ReS estimation and correction, which show improved reflections with less near-surface imprint compared with the input data (Figure 17a). The improvement also is noticeable after the NMO correction of the CMP gathers obtained after the LR-ReS estimation and correction (Figure 18b) when compared with the CMP gathers with statics (Figure 18a) and after residual statics correction with SPM (Figure 18c). Note that our proposed method leads to more continuous events at the near and far offsets in the shallow and deep parts of the CMP gathers as it accounts for the nonsurface-consistent statics. The estimated LR-ReS in the midpoint-offset domain (Figure 16e) shows a pattern similar to the ones obtained from the synthetic data (Figure 8). They are composed of surface-consistent (diagonals at 45°) and nonsurface-consistent statics. The nature of the statics across the line also correlates well with the variations of the elevation profile (Figure 16d).

The complexity of the near-surface weathering layers still leads to a distorted stack after elevation statics correction (Figure 16a). It obtains a minor improvement after the SPM residual statics correction as it only accounts for the surface-consistent statics (Figure 16c). Using the LR-ReS estimation and correction, we obtain a stack section with improved continuity and higher power compared with the other two sections (Figure 16b). The improvement also can be quantitatively assessed using the average stack power (equation 6). The power of the stack after residual statics correction with SPM is 6% higher than that with the elevation statics correction. In contrast, the stack power after our proposed method implemented on data without the NMO correction becomes 17% higher relative to that after the elevation statics correction.

Magnifying the highlighted areas in Figure 16 and autopicking the horizon between 0.55 and 0.6 s confirm the improvement attained with the LR-ReS estimation and correction framework (Figure 19). The autopicked horizons on the stack after the elevation and conventional residual statics corrections suffer due to the imprint of the residual statics that led to erroneous picks. On the contrary, the autopicking process is able to easily pick the horizon after the application of our proposed method, which can provide upgraded interpretation capabilities. Similar to the synthetic data, the estimated LR-ReS can enhance the NMO velocity semblance (Figure 20b), which allows for more confident velocity picking compared with the semblances computed after the elevation and conventional residual statics correction shown in Figure 20a and 20c, respectively. Therefore, by estimating the nonsurface-consistent LR-ReS, we can obtain a more accurate near-surface correction that can lead to substantial improvements.

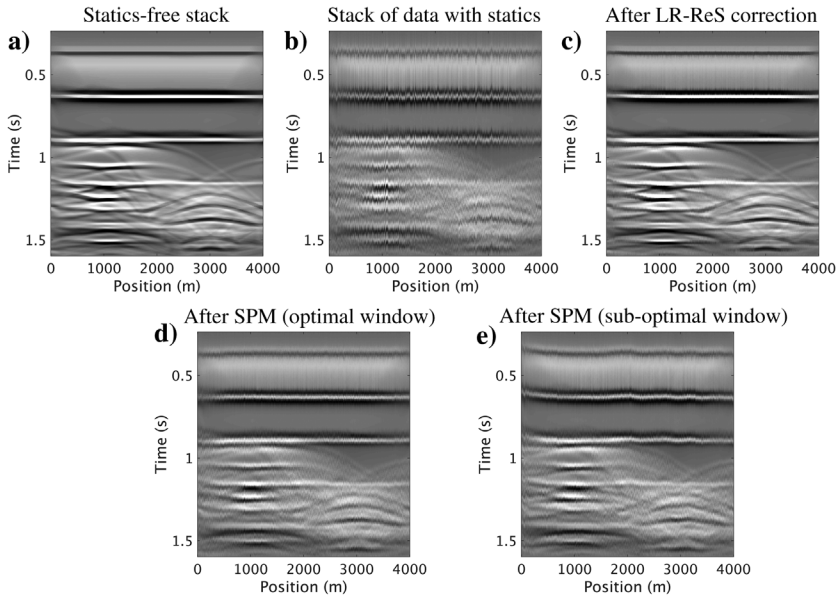

Figure 13. Shot gathers stacks of (a) statics-free data and (b) data affected by short-wavelength statics and data after statics correction with (c) LR-ReS and SPM using (d) an optimal and (e) suboptimal window.

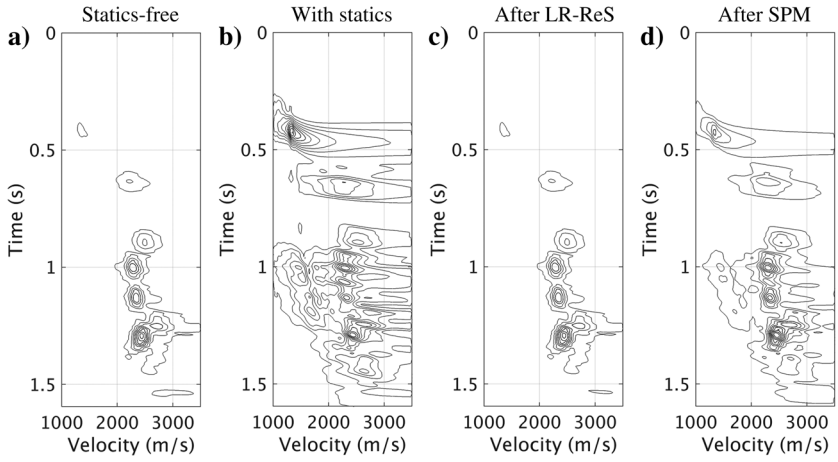

Figure 14. NMO velocity semblances computed from (a) statics-free data and (b) data with statics and data after statics correction with (c) our proposed method and (d) SPM.

DISCUSSION

Using the LR-ReS estimation and correction, we are able to correct for the surface- and nonsurface-consistent statics typically associated with the rapid variations of surface elevation, weathering layers' velocity, and thickness. Removing the surface-consistency assumption can be considered dangerous for the existing nonsurface-consistent techniques such as trim statics (Ursenbach and Bancroft, 2005). In contrast, our proposed method captures the intrinsic relationships between the different midpoints and offsets because it operates on the whole line, i.e., we do not low-rank approximate single gathers. Moreover, LR-ReS estimation and correction do not perform any sort of temporal or spatial windowing to the data, which prevents the statics from becoming biased by certain events. This is the opposite of what other conventional surface- and nonsurface-consistent techniques usually do, i.e., they are dependent on data windowing, which can make them strongly biased (see Figure 13).

The proposed method does not require NMO-corrected gathers for statics estimation. Therefore, short-wavelength statics correction becomes independent of errors in the NMO velocity model. In contrast, the conventional residual statics correction can be affected by errors in the NMO velocity model, which can lead to confusion about whether statics correction, velocity refinement, or both are necessary. The events at approximately 1.2 and 1.5 s of the field data's CMP gathers after the elevation and conventional residual statics correction (Figure 18a and 18b, respectively) may indicate that updating the velocity model is necessary. This also can be noticed from the semblances in Figure 20a and 20c. On the other hand, the CMP gathers after our proposed method, which is not biased by the NMO velocity model as it was applied to the data without the NMO correction, are much less affected by the surface- and nonsurface-consistent statics (Figure 18c). As a result, the NMO velocity model appears to be sufficiently accurate. Moreover, the velocity semblance after the LR-ReS correction is much less affected by the weathering layers compared with that after conventional residual statics correction (Figure 20). In addition, in the presence of a high-velocity layer followed by a lower one, the NMO velocity picking of primaries can be challenged by multiples. In certain situations, the NMO velocity estimation may need to be guided by an interpreter acquainted with the geology. When the velocity semblance is affected by multiples and short-wavelength statics, the NMO velocity estimation can be one of the most efforts- and time-consuming processes in the land seismic data processing. On the contrary, the LR-ReS estimation is independent of the NMO velocity model, which can reduce the multiple iterations of the NMO velocity estimation and short-wavelength statics correction. Therefore, it can increase the overall efficiency of data processing.

Unlike conventional methods that need access to multiple- and noise-free data with aligned primaries after the NMO correction (Cox, 1999; Yilmaz, 2001), which may not always be feasible, the proposed method can be carried out using the total wavefield. If multiples are present in the data even though the selected window for the conventional residual statics correction only contains primaries, the multiples may inadvertently be removed, which can limit the imaging and inversion using primaries and multiples (Verschuur, 2013). Similarly, if the selected window partly contains unaligned multiples, erroneous structures may be introduced (Figure 13e). With the LR-ReS estimation and correction, theprimaries and multiples can be improved as demonstrated by the stacks in the "Results" section. Moreover, the proposed method does not require horizon picking or pilot trace construction, which can be necessary for nonsurface-consistent methods. In the presence of noise or noncontinuous events, these tasks become nontrivial (see Figure 19a and 19c). In contrast, the LR-ReS estimation and correction shows it can correct for the short-wavelength statics on the field data in the presence of noise. Nevertheless, Algorithm 2 requires the selection of two main parameters, which are the ranks $\mathbf{K}$ and frequency bands $\mathbf{f_b}$ that we further elaborate on next.

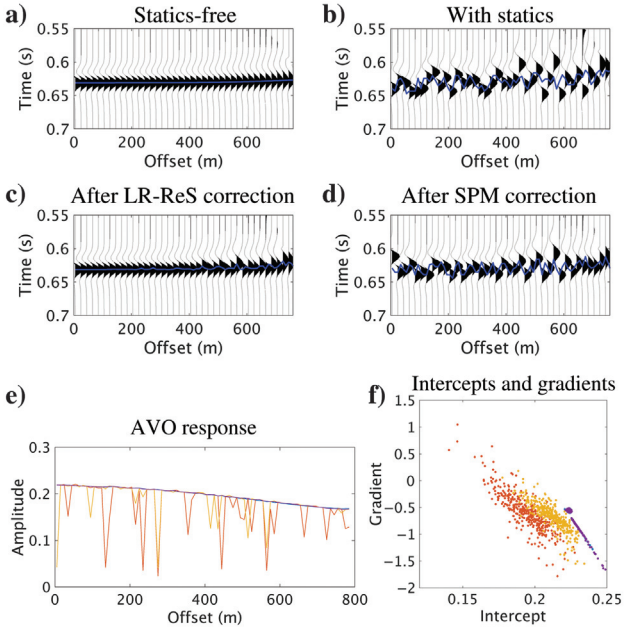

Figure 15. Autopicked AVO responses in the blue lines corresponding to the horizon at 0.65 s for one NMO-corrected CMP gather: (a) statics-free and (b) with statics and after statics correction with (c) LR-ReS and (d) SPM. (e) The AVO responses from the four CMP gathers and (f) intercepts and gradients computed from all CMP gathers at the same horizon that corresponds to the statics-free data (the blue), data with statics (the red), and data after statics correction with LR-ReS (the magenta) and SPM (the yellow).

Practical aspects

We demonstrate the benefits of frequency-band-dependent and multi-rank-scale statics estimation and correction in the "LR-ReS estimation and correction" section. We further clarify some of the practical aspects. For the synthetic and real data, it is sufficient to estimate the statics at three frequency bands spanning low to high frequencies such that we cover the total frequency bandwidth. One way to decide on the frequency bands is to estimate the statics after processing each third of the frequency slices. In practice, the frequency bands at which the statics are estimated will depend on the frequency content of the data set and its quality. For example, the signal-to-noise ratio of the field data below 10.5 Hz and greater than 58 Hz is low. Therefore, we estimate the statics at 25, 40, and 58 Hz.

To select the rank for Algorithms 1 and 2, we linearly increase it with increasing frequency content. This is because higher frequencies contain more variability and therefore require a higher rank for a better low-rank approximation compared with the low frequencies (Figure 4). We note that the rank selection also depends on the complexity of the data, which requires the user's analysis. In

DOI:10.1190/geo2022-0415.1

Algorithm 2, the role of the low-rank approximation is to mitigate the near-surface effect, which we then use in the crosscorrelation for statics estimation. Because we estimate the statics after processing each frequency band rather than each frequency slice, we avoid errors due to low-rank approximation or poor signal-to-noise ratio. Therefore, an error due to the rank selection has less influence on the LR-ReS estimation compared with other rank-based methods that use the rank for explicit output estimation, e.g., Algorithm 1 or rank-minimization problems (equation 3a) usually used for denoising or interpolation. Moreover, using the proposed multi-rank-scale approach alleviates the requirements for accurate low-rank approximation. The strategy of starting with high-rank approximation followed by lower-rank approximation at later iterations results in improved statics estimation as explained in the "LR-ReS estimation and correction" section, which we demonstrate by means of synthetic and field data.

Using more rank scales to estimate the statics at additional frequency bands can add further improvements, e.g., 1–2 dB at certain frequencies of the stack's amplitude spectrum in the shown examples. However, the computational efficiency also depends on these two factors, namely the number of rank scales and frequency bands. The number of rank scales determines the number of SVD computes, whereas the frequency bands determine the number of crosscorrelations. Therefore, the computational

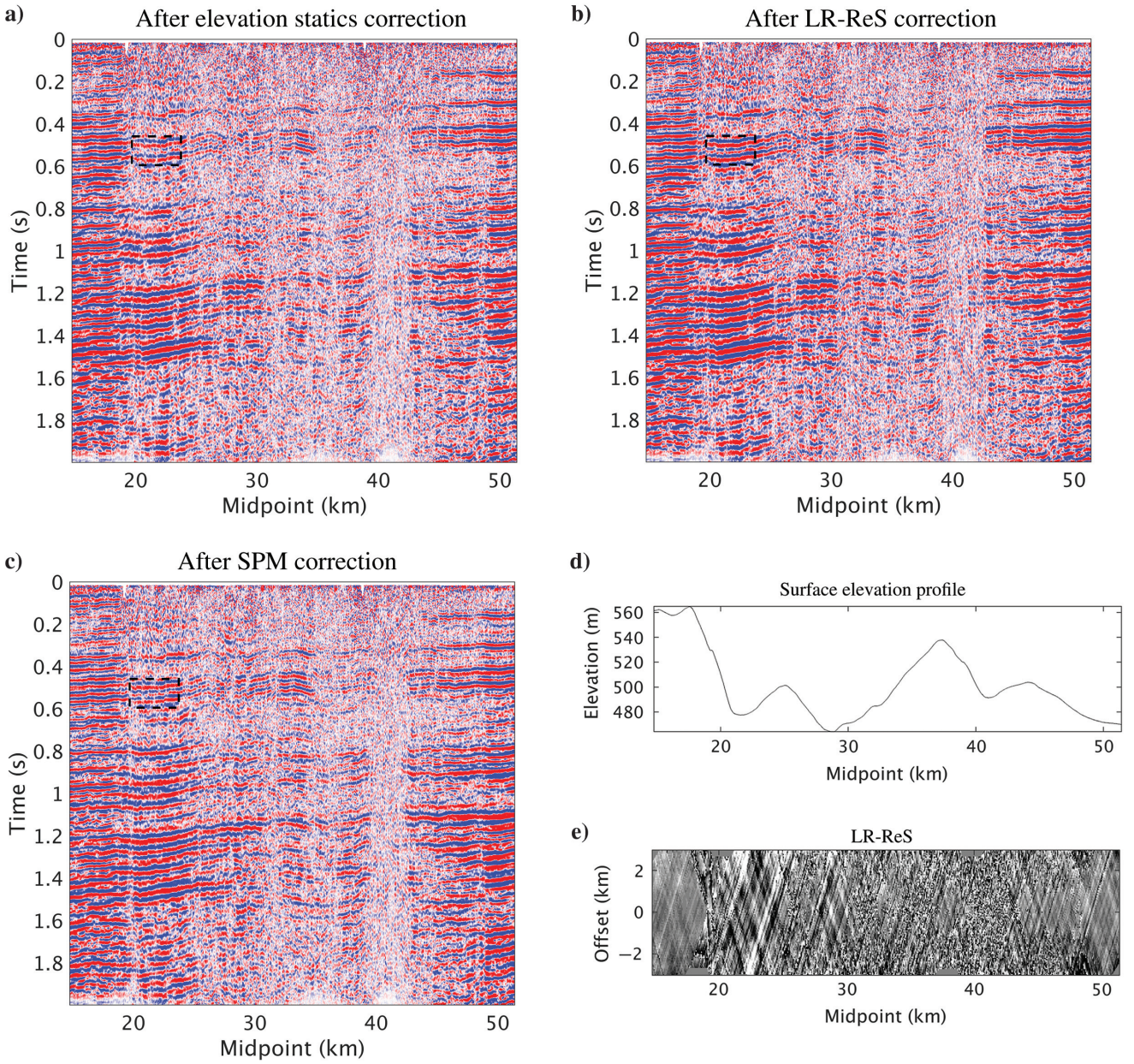

Figure 16. Stack sections of the field data after (a) elevation statics correction, (b) LR-ReS estimation and correction, and (c) residual statics correction with SPM. (d) The average surface elevation profile and (e) the total LR-ReS in the midpoint-offset domain after three rank-scale iterations clipped to ±20 ms.

complexity of the method is determined by the SVD $O(\min\{n_m^2 \times n_h, n_m \times n_h^2\})$, which becomes $O(n_m \times n_h^2)$, as n_h is almost always less than n_m, and crosscorrelations $O(n_t \times n_g)$, where n_g corresponds to the number of crosscorrelation lags. For field and synthetic data, we only compute the SVD three times for each frequency slice. We also estimate the statics at three frequency bands, which requires three crosscorrelations at each rank-scale iteration. The proposed method turns out to be more computationally efficient compared with the residual statics correction with SPM, while at the same time providing better results. Moreover, the efforts- and time-consuming NMO velocity estimation required for conventional methods make our proposed method even more attractive. The computational efficiency of Algorithm 2 can be increased by running it on multiple processors along frequency slices. For large-scale matrices, e.g., in the case of 3D seismic data, SVD can be computationally demanding. Therefore, computation of only a subset of singular vectors along with their corresponding singular values may increase computational efficiency. To further improve the performance of the proposed framework, we mitigate the effect of noise.

Mitigation of the noise effect

We assume that the low-rank structure destruction is due to the effect of the weathering layers, whereas the largest singular values preserve the signal of interest. In reality, more factors may influence the singular values such as the residual ground roll, near-offset noise, and random noise of the field data (Figures 17a and 18a). The singular values of these undesired events become muddled with the larger singular values of the reflections, which influence the performance of low-rank approximation. Consequently, parts of the estimated statics contain the imprint of noise, as shown in Figure 16e. In this case, there is a need for improved preprocessing for ground-roll and noise attenuation, especially because we only apply a simple *f-k* filter and elevation statics correction as pre-processing steps to this challenging field data.

An alternative approach to mitigate the noise effect is to apply an NMO correction, which Trickett and Burroughs (2009) use to minimize the number

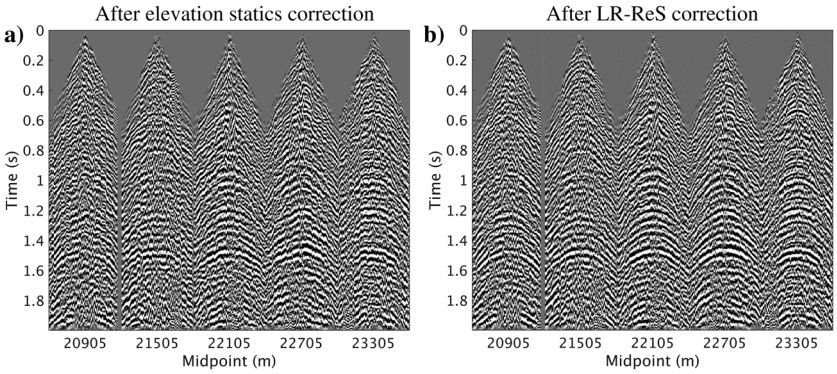

Figure 17. Part of the field data's CMP gathers after (a) elevation statics correction and (b) LR-ReS correction.

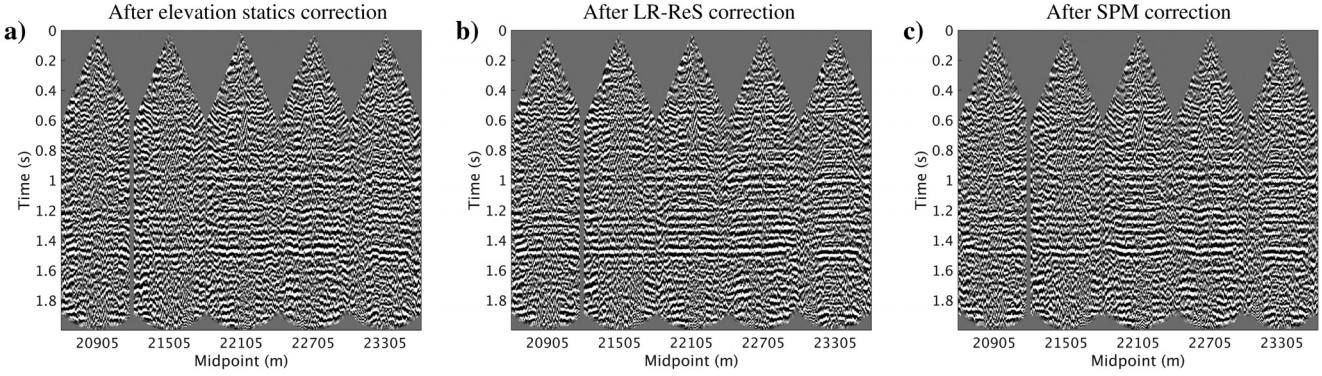

Figure 18. Part of the field data's NMO-corrected CMP gathers after (a) elevation statics correction, (b) LR-ReS correction, and (c) SPM residual statics correction.

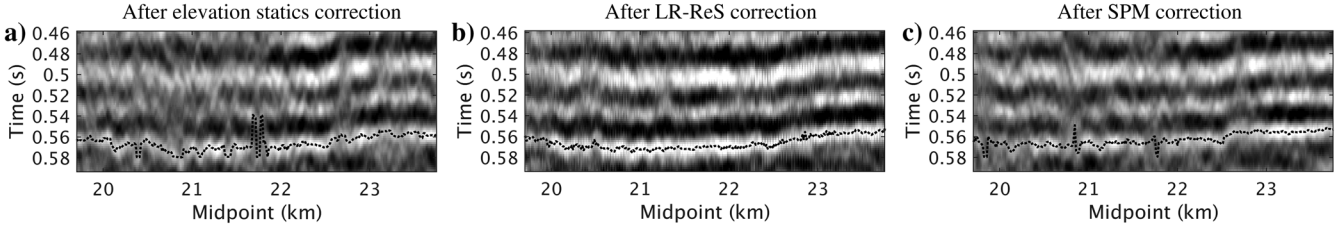

Figure 19. Auto picked horizons (the dotted lines) on the magnification of the field data's stacks at the highlighted areas of Figure 16: (a) before residual statics correction, (b) after LR-ReS correction, and (c) after SPM residual statics correction.

of dipping events and consequently use a smaller rank during denoising with Cadzow filtering. After the NMO correction, aligned reflections in the CMP gathers form most of the events (Figure 18a), which leads the undesired events to be less coherent and consequently exhibit the smaller singular values space. Therefore, the singular values become more rapidly decaying after the NMO correction compared with those without the NMO correction (Figure 21a). As a result, the application of our proposed method on the NMO-corrected data allows for an improved low-rank approximation, which mitigates the effect of noise on the estimated statics and stacks displayed in Figure 22 when compared with those shown in Figures 16b, 16e, and 19b. The obtained stack section and autopicked horizon (Figure 22) show a higher degree of improvement compared with those after the elevation statics and conventional residual statics corrections (Figures 16a, 16c, 19a, and 19c, respectively). The stack power after the residual statics correction with our proposed method becomes 42% higher than that of the data with an elevation statics correction, whereas the improvement with SPM is only 6%. Note that, to achieve the same LR-ReS estimation and correction performance of the data with and without the NMO correction (Figures 16b, 19b, and 22) on these challenging field data, improved preprocessing becomes essential. Even though the data's condition and transform domain without the NMO correction are not optimal, the estimated LR-ReS provides reflections with improved continuity (Figures 17 and 18). Moreover, its stack section (Figure 16b) shows a better performance compared with conventional residual statics correction (Figure 16c), which requires NMO velocity estimation and correction.

In contrast to the field data, the synthetic data set is ideal, except for the added short-wavelength statics. Therefore, removing the direct wavefield and part of the reflected wavefield imposed by the NMO correction can decrease the redundancy of the data and influence the singular values decay. To observe that, we examine the singular values decay prior to the LR-ReS correction on the data with and without the NMO correction (Figure 21b). We notice that the NMO correction results in a slower singular values decay compared with the data without the NMO correction due to the applied mute. In this case, the midpoint-offset domain without the NMO correction is the better one for statics estimation.

We indicate that the conventional surface- and nonsurface-consistent residual statics estimation methods can be influenced by noise. In this case, surface-consistent statics can provide a more stable solution compared with nonsurface-consistent ones. For the shown field data set, which is contaminated with noise, it is not necessary to enforce surface consistency. However, if a surface-consistent solution is desired, it can be computed by averaging the estimated statics along the rows and columns in the source-receiver domain.

Further extensions and applications

Residual statics correction usually compensates for the short-wavelength component of the statics. Therefore, we assume that the data can be redatumed to a flat surface (roughly) using long-wavelength statics correction methods, after which the residual statics correction can be applied. To apply the LR-ReS estimation and correction to the field data with varying topography prior to the long-wavelength statics correction, further tests need to be carried out. We envision that if the near surface renders the coherent energy incoherent and the largest singular values preserve the coherent energy, LR-ReS estimation and correction can still be applicable.

As evident from the field data stack (Figure 16a), the data set is affected by various near-surface conditions. Between 15 and 18.5 km as well as between 43 and 52 km, there is a minor distortion due to the near surface. As a result, only the small LR-ReS is estimated (Figures 16e and 22a). Most of the improvement is obtained between 18.5 and 40 km (Figures 16b and 22b). On the other hand, between 40 and 43 km, the data set is heavily distorted and exhibits

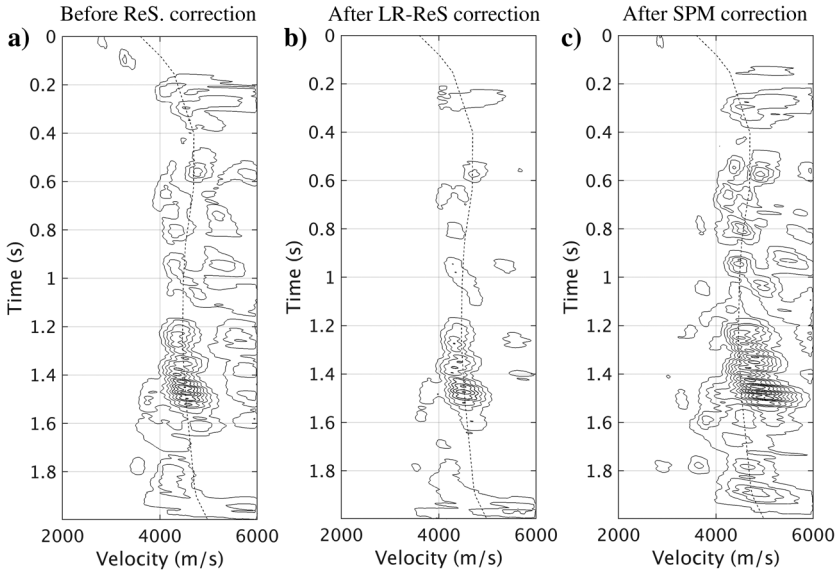

Figure 20. NMO velocity semblances computed from CMP gathers of the field data (a) before residual statics (ReS) correction, (b) after LR-ReS correction, and (c) after SPM residual statics correction. The dashed lines show the originally picked NMO velocity.

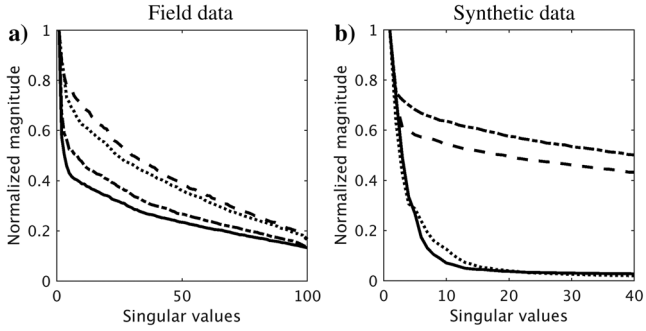

Figure 21. The largest singular values computed from the frequency slices in the midpoint-offset domain of (a) field data and (b) synthetic data without NMO correction (the dashed curves), with NMO correction (the dashed-dotted curves), and after LR-ReS estimation and correction of data without (the dotted curves) and with (the solid curves) NMO correction.

no coherency due to the near-surface conditions and the 3D effects not captured by the 2D data. In this case, a 3D wave-equation-based solution is necessary to overcome the limitations of the elevation statics correction, which can be followed by the LR-ReS estimation and correction.

The proposed LR-ReS estimation and correction framework is currently implemented on 2D data. However, it can be easily extended to three dimensions, where the 5D data volume becomes parameterized by midpoints and offsets along the x- and y-dimensions (m_x, m_y and h_x, h_y), respectively. Other tensor- or matrix-based transform-revealing parameterizations also can be used. The inclusion of multidimensional data can further benefit LR-ReS estimation by increasing the redundancy of the data, which can lead to better performance compared with processing separate 2D lines. However, poor sampling with coarse sources and receivers may prevent that if the few largest singular values do not capture the coherent energy. We note that there can be a difference between the field data grid and the computational grid. In the shown field data example, we place the CMP gathers at the grid points nearest to the actual field positions. After statics estimation and correction, the traces can be sorted back to the original domain. Therefore, a further point of research can be related to the binning of off-the-grid data. Currently, the estimated LR-ReS is offset-variant, which can be the case when raypaths in the near surface diverge from the normal incidence. The statics also may become time variant, which requires additional analysis to implement the LR-ReS estimation and correction in this situation.

A potential application of the LR-ReS estimation and correction is S-wave short-wavelength statics correction, as the proposed method can estimate large statics with the frequency-band-dependent approach. In addition to using residual statics correction in conventional processing workflows, it also can be used as a preprocessing step prior to full wavefield imaging and inversions such as full-waveform inversion and joint migration inversion (Tarantola, 1984; Virieux and Operto, 2009; Berkhout, 2014) as residual statics can be beyond the resolution of these methods. Or even better, residual statics correction should be combined together with these dynamic processes to explain the whole data and obtain more complete near- and subsurface models. Alfaraj and Verschuur (2020) show initial steps in this direction. Not requiring an NMO velocity model and being able to correct for the surface- and nonsurface-consistent short-wavelength statics make the LR-Res estimation and correction more favorable compared with the existing methods.

CONCLUSION

The surface-consistency assumption commonly used in short-wavelength statics correction can be successful on many occasions. However, when raypaths in the near surface diverge from the normal incidence, residual statics correction with SPM can be shown to fail to fully correct for short-wavelength statics. In this case, an additional nonsurface-consistent statics correction process is required, which adds to the computational costs and can be prone to errors in the presence of noise or when picking noncontinuous horizons. To overcome these limitations, we propose an LR-ReS estimation and correction framework that can simultaneously correct for the surface- and nonsurface-consistent statics. The method uses the redundant nature of midpoint-offset frequency slices to iteratively estimate the multi-rank-scale and frequency-band-dependent statics. The proposed LR-ReS estimation and correction can estimate short-wavelength statics without the need for the NMO correction, which can reduce the efforts- and time-consuming multiple passes of the NMO velocity estimation and residual statics correction. Consequently, it also does not require windowing over a noise-free area containing primaries or windowing to avoid the NMO stretch effect. Results on synthetic and field data show significant improvements that conventional residual statics correction could not achieve. Because the method can be directly applied to the total

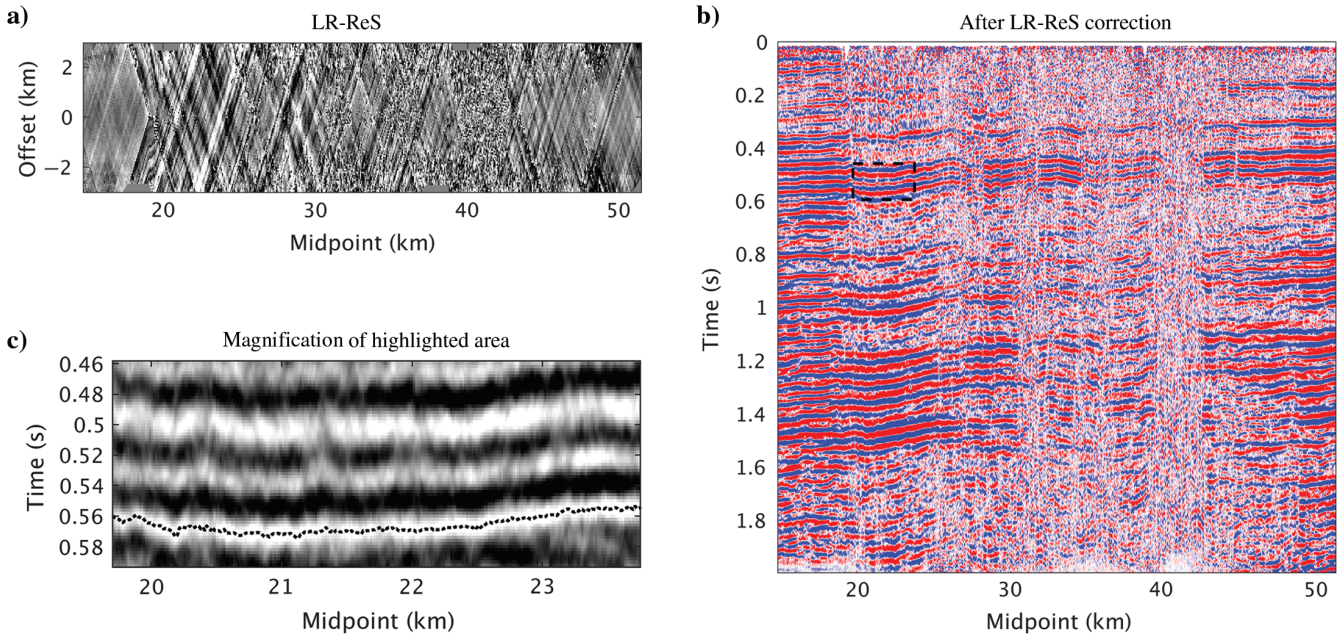

Figure 22. (a) The total estimated statics in the midpoint-offset domain clipped to ±20 ms, (b) stack, and (c) magnified at the highlighted area of (b) with the autopicked horizon after the LR-ReS correction of NMO-corrected data.

wavefield without extensive preprocessing, e.g., multiple removal and NMO velocity estimation, residual statics correction becomes feasible prior to the other processing steps to improve their performance. Further potential applications include short-wavelength statics correction prior to first-breaks picking, traveltime inversion, or full wavefield imaging and inversion techniques. These findings make the proposed method preferable to correct for short-wavelength statics compared with the conventional methods.

ACKNOWLEDGMENTS

A. M. Alfaraj extends his gratitude to Saudi Aramco for sponsoring his Ph.D. studies. We also would like to thank Saudi Aramco for providing the field data.

DATA AND MATERIALS AVAILABILITY

Data associated with this research are confidential and cannot be released.

REFERENCES

Al-Ali, M., and D. Verschuur, 2006, An integrated method for resolving the seismic complex near-surface problem: Geophysical Prospecting, **54**, 739–750, doi: 10.1111/j.1365-2478.2006.00575.x.

Alfaraj, A., M. Almubarak, and F. Herrmann, 2019, Correcting for short-wavelength statics with low rank approximation: 81st Annual International Conference and Exhibition, EAGE, Extended Abstracts, doi: 10.3997/2214-4609.201901205.

Alfaraj, A., and E. Verschuur, 2020, Mitigating the near-surface effect in velocity and reflectivity estimation with multi-scale low-rank approximated image updates: 82nd Annual International Conference and Exhibition, EAGE, Extended Abstracts, doi: 10.3997/2214-4609.202011619.

Alfaraj, A. M., R. Kumar, and F. J. Herrmann, 2018, Automatic statics and residual statics correction with low-rank approximation: 80th Annual International Conference and Exhibition, EAGE, Extended Abstracts, doi: 10.3997/2214-4609.201801107.

Aravkin, A., R. Kumar, H. Mansour, B. Recht, and F. J. Herrmann, 2014, Fast methods for denoising matrix completion formulations, with applications to robust seismic data interpolation: SIAM Journal on Scientific Computing, **36**, S237–S266, doi: 10.1137/130919210.

Bekara, M., and M. Van der Baan, 2007, Local singular value decomposition for signal enhancement of seismic data: Geophysics, **72**, no. 2, V59–V65, doi: 10.1190/1.2435967.

Berkhout, A., 2014, An outlook on the future of seismic imaging, Part III: Joint migration inversion: Geophysical Prospecting, **62**, 950–971, doi: 10.1111/1365-2478.12158.

Breuer, A., N. Ettrich, and P. Habelitz, 2020, Deep learning in seismic processing: Trim statics and demultiple: 90th Annual International Meeting, SEG, Expanded Abstracts, 3199–3203, doi: 10.1190/segam2020-3427887.1.

Candes, E., L. Demanet, D. Donoho, and L. Ying, 2006, Fast discrete curvelet transforms: SIAM Journal on Multiscale Modeling and Simulation, **5**, 861–899, doi: 10.1137/05064182X.

Chen, Y., Y. Zhou, W. Chen, S. Zu, W. Huang, and D. Zhang, 2017, Empirical low-rank approximation for seismic noise attenuation: IEEE Transactions on Geoscience and Remote Sensing, **55**, 4696–4711, doi: 10.1109/TGRS.2017.2698342.

Cheng, J., and M. D. Sacchi, 2015, Separation and reconstruction of simultaneous source data via iterative rank reduction: Geophysics, **80**, no. 4, V57–V66, doi: 10.1190/geo2014-0385.1.

Chopra, S., and J. P. Castagna, 2014, AVO: SEG.

Cox, M., 1999, Static corrections for seismic reflection surveys: SEG.

Dukalski, M., D. Rovetta, S. van der Linde, M. Moller, N. Neumann, and F. Phillipson, 2022, Quantum computer-assisted global optimization in geophysics illustrated with stack power maximization for refraction residual statics estimation: Geophysics, **88**, no. 2, 1–74, doi: 10.1190/geo2022-0253.1.

Eckart, C., and G. Young, 1936, The approximation of one matrix by another of lower rank: Psychometrika, **1**, 211–218, doi: 10.1007/BF02288367.

Gholami, A., 2013, Residual statics estimation by sparsity maximization: Geophysics, **78**, no. 1, V11–V19, doi: 10.1190/geo2012-0035.1.

Gholami, A., 2014, Phase retrieval through regularization for seismic problems: Geophysics, **79**, no. 5, V153–V164, doi: 10.1190/geo2013-0318.1.

Golub, G. H., and C. Reinsch, 1971, Singular value decomposition and least squares solutions: Numerische Mathematik, **14**, 403–420.

Henley, D. C., 2012, Interferometric application of static corrections: Geophysics, **77**, no. 1, Q1–Q13, doi: 10.1190/geo2011-0082.1.

Kreimer, N., and M. D. Sacchi, 2012, A tensor higher-order singular value decomposition for prestack seismic data noise reduction and interpolation: Geophysics, **77**, no. 3, V113–V122, doi: 10.1190/geo2011-0399.1.

Kumar, R., C. Da Silva, O. Akalin, A. Y. Aravkin, H. Mansour, B. Recht, and F. J. Herrmann, 2015, Efficient matrix completion for seismic data reconstruction: Geophysics, **80**, no. 5, V97–V114, doi: 10.1190/geo2014-0369.1.

Maraschini, M., R. Dyer, K. Stevens, and D. Bird, 2012, Source separation by iterative rank reduction — Theory and applications: 74th Annual International Conference and Exhibition, EAGE, Extended Abstracts, doi: 10.3997/2214-4609.20148370.

Marsden, D., 1993, Static corrections — A review, Part II: The Leading Edge, **12**, 115–120, doi: 10.1190/1.1436936.

Moldoveanu, N., 2011, A singular value decomposition algorithm for the attenuation of high energy towed-streamer noise: First Break, **29**, 101–108, doi: 10.3997/1365-2397.29.12.55902.

Oropeza, V., and M. Sacchi, 2011, Simultaneous seismic data denoising and reconstruction via multichannel singular spectrum analysis: Geophysics, **76**, no. 3, V25–V32, doi: 10.1190/1.3552706.

Ronen, J., and J. F. Claerbout, 1985, Surface-consistent residual statics estimation by stack-power maximization: Geophysics, **50**, 2759–2767, doi: 10.1190/1.1441896.

Sheriff, R. E., 2002, Encyclopedic dictionary of applied geophysics, 4th ed.: SEG.

Stanton, A., N. Kazemi, and M. D. Sacchi, 2013, Processing seismic data in the presence of residual statics: 83rd Annual International Meeting, SEG, Expanded Abstracts, 1838–1842, doi: 10.1190/segam2013-1453.1.

Taner, M. T., F. Koehler, and K. A. Alhilali, 1974, Estimation and correction of near-surface time anomalies: Geophysics, **39**, 441–463, doi: 10.1190/1.1440441.

Tarantola, A., 1984, Inversion of seismic reflection data in the acoustic approximation: Geophysics, **49**, 1259–1266, doi: 10.1190/1.1441754.

Thorbecke, J. W., and D. Draganov, 2011, Finite-difference modeling experiments for seismic interferometry: Geophysics, **76**, no. 6, H1–H18, doi: 10.1190/geo2010-0039.1.

Trickett, S., and L. Burroughs, 2009, Prestack rank-reduction-based noise suppression: CSEG Recorder, **34**, 24–31.

Trickett, S., L. Burroughs, A. Milton, L. Walton, and R. Dack, 2010, Rank-reductionbased trace interpolation: 80th Annual International Meeting, SEG, Expanded Abstracts, 3829–3833, doi: 10.1190/1.3513645.

Trickett, S. R., 2003, *F-xy* eigenimage noise suppression: Geophysics, **68**, 751–759, doi: 10.1190/1.1567245.

Ulrych, T. J., S. Freire, and P. Siston, 1988, Eigenimage processing of seismic sections: 58th Annual International Meeting, SEG, Expanded Abstracts, 1261–1265, doi: 10.1190/1.1892508.

Ursenbach, C. P., and J. C. Bancroft, 2005, Playing with fire: Noise alignment in trim and residual statics: 75th Annual International Meeting, SEG, Expanded Abstracts, 1973–1976, doi: 10.1190/1.1816525.

Verschuur, D. J., 2013, Seismic multiple removal techniques: Past, present and future (revised edition): EAGE Publications.

Virieux, J., and S. Operto, 2009, An overview of full-waveform inversion in exploration geophysics: Geophysics, **74**, no. 6, WCC1–WCC26, doi: 10.1190/1.3238367.

Wason, H., R. Kumar, F. J. Herrmann, and A. Y. Aravkin, 2014, Source separation via SVD-free rank minimization in the hierarchical semi-separable representation: 84th Annual International Meeting, SEG, Expanded Abstracts, 120–126, doi: 10.1190/segam2014-1583.1.

Xu, J., H. Zhang, and J. Zhang, 2018, A robust surface-consistent residual phase correction method based on migrated gathers: Exploration Geophysics, **49**, 336–344, doi: 10.1071/EG17017.

Yilmaz, O., 2001, Seismic data analysis: SEG.

Zhang, M., Y. Liu, H. Zhang, and Y. Chen, 2020, Incoherent noise suppression of seismic data based on robust low-rank approximation: IEEE Transactions on Geoscience and Remote Sensing, **58**, 8874–8887, doi: 10.1109/TGRS.2020.2991438.

Biographies and photographs of the authors are not available.